UNIVERSITY OF VAASA

FACULTY OF TECHNOLOGY

TELECOMMUNICATIONS ENGINEERING

Tibebu Sime

EQUALIZATION OF MIMO CHANNELS IN LTE-ADVANCED

Master's thesis for the degree of Master of Science in Technology submitted for inspection on 2nd July 2012 in Vaasa.

Supervisor Prof. Mohammed Elmusrati

Instructor Mr. Mulugeta Fikadu

ACKNOWLEDGEMENT

It gives me a great pleasure to thank everyone who supported me in any respect to write my thesis successfully.

First of all, I am profoundly honored and exceedingly humbled to thank my supervisor Professor Mohammed Elmusrati and my advisor Mr. Mulugeta Fikadu without whose uninterrupted guidance, the completion of this thesis would not have been possible. They both helped me choose my title –which is one of the most important and widely researched topics in modern broadband wireless mobile accesses –and provided me with constructive ideas throughout this thesis.

Secondly, I owe sincere and earnest gratitude to all Tritonia Library staff members at the University of Vaasa for allowing me to borrow the references which enabled me to develop an understanding of the subject at any time I needed them.

I am also truly indebted and grateful to Smedsby Bokfix for their remarkable cooperation in printing the thesis after it was submitted for inspection and finally approved.

Last but by no means least, I am obliged to offer regards and blessings to my mother Bilile Fayisa and my father Abebe Sime whose sacrifice , never-ceasing love and support has given me the strength to persevere to the end; my sisters Dinkenesh A. Sime, Tsehay A. Sime and my brother Abdisa A. Sime for having been on my side in boosting me morally; and my best friends Mr. Rao Sikha, Mr. Zakarias Ondit, Mr. Seyoum Nerisho , Mr. Bahiru Gemeda and Mr. Samuel Ailen-Ubhi for encouraging and providing me with a pool of information resources till I put the final full stop to this paper.

Glory to God!!!

Tibebu Sime

University of Vaasa, Finland, July 2012.

Table of Contents

LIST OF ABBREVIATIONS

2G	2nd Generation
3G	3rd Generation
3GPP	3rd Generation Project Partnership
4G	4th Generation
ADC	Analog-to-Digital Converter
ADSL2+	Evolved Asymmetric Digital Subscriber Line
AWGN	Additive White Gaussian Noise
BER	Bit Error Rate
CCDF	Complementary Cumulative Distribution Function
CDF	Cumulative Distribution Function
CDMA	Code Division Multiple Access
CLT	Central Limit Theorem
DAC	Digital-to-Analog Converter
DFDMA	Distributed Frequency Division Multiple Access
DFT	Discrete Fourier Transform
DL	Downlink
eNodeB	enhanced NodeB
E-UTRA	Evolved UMTS Terrestrial Radio Access
FDD	Frequency Division Multiplexing
FFT	Fast Fourier Transform
GPON	Gigabit Passive Optical Network
GSM	Global System for Mobile Communications
HSDPA	High Speed Downlink Packet Access
HSPA+	Evolved High Speed Packet Access

IFFT	Inverse FFT
IMT	International Mobile Telecommunications
LFDMA	Localized Frequency Division Multiple Access
ITU	International Telecommunications Union
LTE	Long-Term Evolution
MIMO	Multiple Input Multiple Output
MISO	Multiple Input Single Output
MMSE	Minimum Mean Square Error
MRC	Maximum Ratio Combining
MU-MIMO	Multi-User MIMO
OFDMA	Orthogonal Frequency Division Multiple Access
P/S	Parallel-to-Serial Converter
PAPR	Peak-to-Average Power Ratio
PDF	Probability Density Function
QAM	Quadrature Amplitude Modulation
QPSK	Quadrature Phase Shift Keying
RF	Radio Frequency
rms	root mean square
RNC	Radio Network Controller
S/P	Serial-to-Parallel Converter
SAE	System Architecture Evolution
SC-FDMA	Single Carrier Frequency Division Multiple Access
SIMO	Single Input Multiple Output
SINR	Signal-to-Interference plus Noise Ratio
SISO	Single Input Single Output

SNR	Signal-to-Noise Ratio
SQNR	Signal-to-Quantization-Noise Ratio
SU-MIMO	Single User MIMO
SVD	Singular Value Decomposition
TDD	Time Division Multiplexing
TDMA	Time Division Multiple Access
UE	User Equipment
UL	Uplink
UMTS	Universal Mobile Telecommunications System
VDSL2	Very High Data Subscriber Line
WCDMA	Wideband CDMA
WiMAX	Worldwide Interoperability for Microwave Access
ZF	Zero Forcing
ZF-SIC	Zero Forcing Successive Interference Cancellation

UNIVERSITY OF VAASA
Faculty of Technology
Author: Tibebu Sime
Topic of the Thesis: Equalization of MIMO Channels in LTE- Advanced
Supervisor: Prof. Mohammed Elmusrati
Instructor: Mr. Mulugeta Fikadu
Degree: Master of Science in Technology
Department: Department of Computer Science
Degree program: Degree Program in Telecommunications Engineering
Major Subject: Telecommunications Engineering
Year of Entering the University: 2010
Year of Completing the Thesis: 2012 **Pages: 95**

Abstract

LTE-Advanced is one of the most evolving and competing standards that target the high speed 4G wireless communications. In order to meet the target of this new cellular technology developed under auspices of the 3GPP standardization bodies, it is necessary to ensure that this technology is able to provide the headline requirements recommended for the terrestrial components of the IMT-Advanced radio interface for 4G broadband mobile communications. One of the key radio technologies that will enable LTE-Advanced to achieve the high data throughput rates is the use of MIMO antennas that play an important role as the conventional communications like using more bandwidths and higher modulation types are limited. Together with this are the downlink OFDMA and the uplink SC-FDMA techniques that are employed to improve the system architecture burdened with the data rates rising pretty well above what was previously in use. The combination of these technologies will help LTE-Advanced keep pace with other wireless technologies that may be competing to offer very high data rates and high level of mobility. But achieving the high data rate up to 1 Gbits/s in 4G mobile networks over wide frequency bandwidths and recovering the original information without being corrupted and downgraded has been a daunting task for engineers. Thus, this paper will briefly discuss the performances of MIMO equalization techniques such as MMSE, ZF and ZF-SIC equalizers in a Rayleigh multichannel fading.

KEYWORDS: LTE, LTE-Advanced, MIMO, Rayleigh channel, OFDMA, SC-FDMA

1. INTRODUCTION

It is generally believed that one of the greatest achievements of telecommunication industry in the 21st Century is not only the innovation of sophisticated individual devices, but also the integration of a number of existing technologies into new systems which effectively use their component parts, and the interoperability between heterogeneous technologies which make communications accessible everywhere. Indeed, it was during the last decade that the integrations between these different technologies have become practical. Nevertheless, in spite of some problems associated with introducing this new system, broadband wireless mobile access networks have already proved incredibly successful throughout the world, and 4G mobile networks will be commercially deployed in 2013 to provide a considerable amount of data rate up to 1 Gbits/s in a pedestrian channel environment, which customers have been craving for.

Thus, in response to the increasing demand for maximum data rate and the desire to upgrade the status quo, an efficient radio resource management in cellular networks which makes use of the finite available resources and the techniques to exploit spatial multiplexing MIMO channels have been the fundamental objectives of a good engineering design.

According to Cisco Visual Networking Index (2010), global mobile data traffic is predicted to double every year through 2014. This forest has shown that users will require high throughput with low latency to support real-time applications such as voice calls, gaming and mobile video-conference. Luckily enough, pre-commercial trials of LTE-Advanced have already proved the capacity of this technology to fulfill such high requirements.

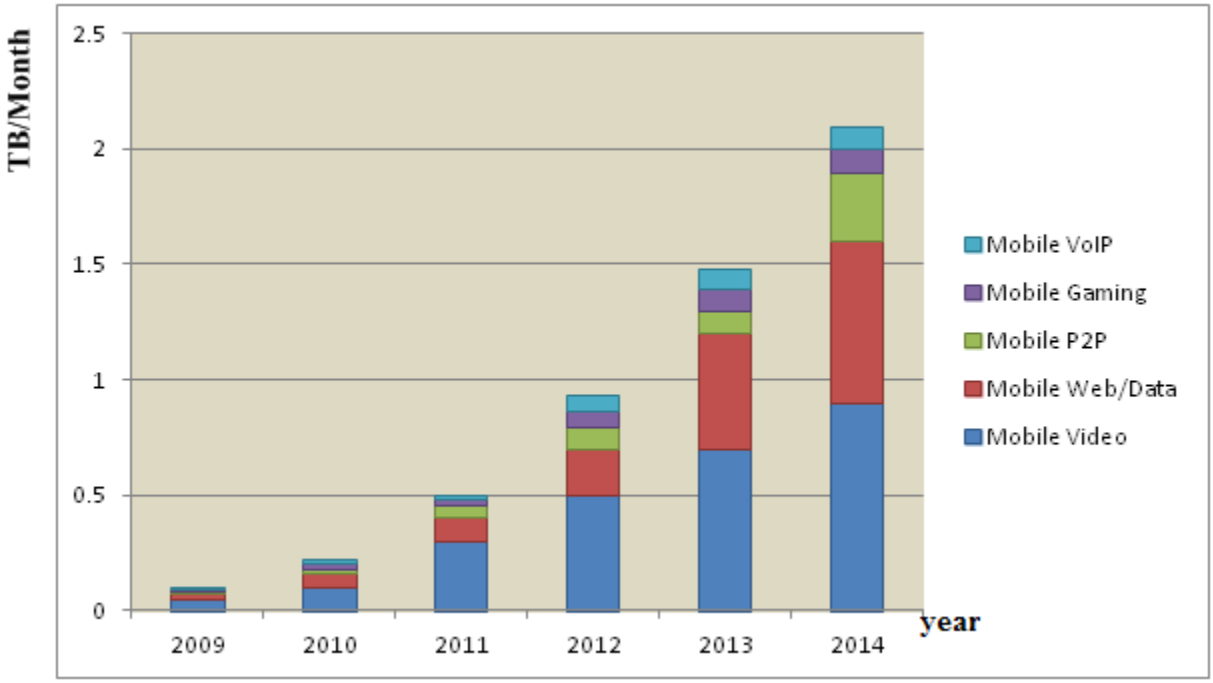

Figure 1.1. Forecast for mobile data traffic.

As can been seen in the above figure, mobile video will generate most of the global mobile data traffic through 2014 because it is obvious that the content of mobile video has higher bit rates than that of the others.

1.1. High Speed Wireless Communications: LTE and Its Advanced Version

In 2G mobile networks, for instance GSM, the user data capability was not the core of the network planning design as the network was dominated by the voice traffic. But with mobile networks covering the majority of the world's population, the demand for high speed broadband data applications including video streams , mobile TV , online gaming ,

internet access and file sharing dramatically increased. On this account, the introduction of 3G networks with HSDPA has significantly boosted the data usage.

The demand for a higher performance of broadband wireless technology did not stop there since the wireline technologies like GPON, VDSL2 and ADSL2+ have also kept on improving the capacity of the service. Hence, the initiatives to work toward the 3GPP LTE and its advanced version in the wireless industry were conceived in 2004 and 2009, respectively to win over the competitions from these wireline communications (Holma & Toskala 2009: 2-11).

According to Wireless Research and Analysis' (Maravedis 2010) forecasts , with this substantial momentum , LTE mobile communications will become the most accepted standard for 4G systems ,and have been estimated to have over 200 million subscribers by 2015. It is also expected a migration of WiMAX operators towards LTE anytime soon before the commercial deployment of LTE-Advanced which promises further performance and this is one of the reasons why 3GPP LTE is going to win the 4G-battle over the IEEE802.16m WiMAX.

Moreover, the seamless interoperability capability of LTE with the legacy systems (3GPP-based 2G/3G networks and 3GPP2-based 2G/3G networks) has made it popular among the service providers as this will allow them to roll out their LTE network in several phases without interrupting the existing services.

Meanwhile in response to the ITU requirements for IMT-Advanced systems circular letter inviting candidate radio interface technologies, 3GPP created a technical report summarizing LTE-Advanced requirements in the *Technical Specification Group Radio Access Network: Requirements for Further Advancements for E-UTRA LTE-Advanced* (Agilent Technologies 2011; Nakamura 2009). These include:

- High degree of commonality of function worldwide while retaining the flexibility to support a wide range of services and applications in a cost efficient manner;
- Compatibility of services within IMT and with fixed networks;

- Capability of internetworking with other radio access networks;
- High quality mobile services;
- User equipment suitable for worldwide use;
- User-friendly applications , services and equipment ;
- Worldwide roaming capability ; and
- Enhanced peak data rate to support advanced services and applications in both low and high mobility environments.

Then the detail of the main technical specifications for LTE and LTE-Advanced is summarized in the following table.

Table 1.1. Main technical specification for LTE and LTE-Advanced.

Performance Indicators	**LTE** **Release 8**	**LTE-Advanced** **Release 10**
Peak data rate	DL: 300 Mb/s(8×8 antennas)	1 Gb/s (8×8 antennas)
	UL: 75 Mb/s (4×4 antennas)	500 Mb/s (4×4 antennas)
Peak spectrum efficiency (bps/Hz)	DL: 15 (8×8 antennas)	30 (8×8 antennas)
	UL: 3.75 (4×4 antennas)	15 (4×4 antennas)
Control plane latency (Handover)	<100 ms	<50 ms
User plane latency (Link layer)	<5 ms	About 1 ms
Duplex mode	FDD and TDD	FDD and TDD
VoIP capacity	200 active users /cell/5MHz	3x higher than that in LTE
Transmission bandwidth	1.4,3,5,10,15,& 20 MHz	up to 100 MHz
User mobility	10 –350 km	350 –500 km

Physical layer access scheme	DL: OFDMA	OFDMA
	UL: SC-FDMA	SC-FDMA
Cell spectrum efficiency (throughput) (bps/Hz/cell)	DL: 2×2 1.69	2.4
	4×2 1.87	2.6
	4×4 2.67	2.7
	UL: 1×2 0.735	1.2
	2×4 -	2.0
Cell edge spectrum efficiency (throughput) (bps/Hz/cell/user)	DL: 2×2 0.05	0.07
	4×2 0.06	0.09
	4×4 0.08	0.12
	UL: 1×2 0.024	0.04
	2×4 -	0.07
Modulation order	QPSK,16-QAM,64-QAM	QPSK,16-QAM,64-QAM
Subcarrier spacing	15 kHz	15 kHz
CP length	Short : 4.7μs	4.7μs
	Long: 16.7μs	16.7μs
Coverage	up to 30 km	up to 100 km

1.2. LTE Standardization Process

In reference to Holma et al. (2009:13-20); 3GPP Releases (2012), the development of LTE Standards by 3GPP standardization body will be summarized in the following table. It is a process which elaborates how LTE-Advanced comes into being.

Table 1.2. LTE standardization phase.

Event in stage	**Release**	**Cellular Technology**
Nov. 2004- 3GPP began a project to define LTE of UMTS cellular technology	-	-
Sep. 2005-Stage 1 (freeze) Sep. 2006-Stage 2 (freeze) Dec. 2007-Stage 3 (freeze)	3GPP Release 7	HSPA+ standard
Mar. 2008-Stage 1 (freeze) June 2008- Stage 2 (freeze) Dec. 2008 -Stage 3 (freeze)	3GPP Release 8	LTE standard
Dec. 2008- Stage 1 (freeze) June 2009-Stage 2 (freeze) Dec. 2009-Stage 3 (freeze)	3GPP Release 9	SAE enhancements , WiMAX and UMTS interoperability
Mar. 2010-Stage 1 (freeze) Sep. 2010-Stage 2 (freeze) Mar. 2011-Stage 3 (freeze)	3GPP Release 10	LTE-Advanced

It can be noted from the content of the above table that 3GPP standards are typically released in three stages. *Stage 1* introduces the standard description from standard's user point of view, followed by *Stage 2* in which a logical analysis, breaking the problem down into functional elements and the information flows amongst them are described. Finally, *Stage 3* presents the concrete implementation of the protocols between the physical elements onto which the functional elements have been mapped.

1.3. 3GPP Standardization Bodies

3GPP is a collaboration agreement that was established and formalized in December 1998 to bring together a number of regional and national telecommunication standardization bodies which are known as *Organizational Partners* which determine the general policy and strategy of 3GPP and perform the following tasks according to 3GPP Partners (2012):

- Approval and maintenance of the 3GPP scope and Partnership Project Description ;
- Taking decisions on the creation or cessation of Technical Specification Groups (PSTs), and approving their scope and terms of reference;
- Approval of Organizational Partners funding requirements ;
- Allocation of human and financial resources provided by the Organizational Partners to the Project Coordination Group(PCG) ; and
- Acting as a body of appeal on procedural matters referred to them.

Organizational Partners is the union of six telecommunication standard bodies which have come from Asia, Europe and North America. These are:

1. ARIB (Japan)-Association of Radio Industries and Businesses
2. ATIS (USA)-Alliance for Telecommunications Industry Solutions
3. CCSA (China)-China Communications Standards Association
4. ETSI (Europe)-European Telecommunications Standards Institute
5. TTA (South Korea)-Telecommunications Technology Association
6. TTC (Japan)-Telecommunications Technology Committee

Together with the Organizational Partners, there are currently 12 *Market Representation Partners* which provide for the maintenance of the Partnership Project Agreement, the approval of applications for 3GPP partnership and taking decisions related to the dissolution of 3GPP. These are: IMS Forum, GSA, GSM Association IPv6 Forum, 3G

Americans, TD-SCMA Industry Alliance, Info Communication Union, Femto Forum, CDMA Development Group, Cellular Operators Association of India and UMTS Forum. (3GPP Partners 2012.)

In addition to the two partners, there are three observers which are *Standards Development Organizations* which are qualified to become future Organizational Partners. These are:

1. TIA (USA)-Telecommunications Industries Association
2. ISACC (Canada)-ICT Standards Advisory Council of Canada
3. CA (Australia)-Communications Alliance

3GPP has also got tremendous support from various vendors and operators which have come together to facilitate the LTE standard setting by providing recommendations and feedback by knowledge gathered during trials. These include *Next Generation Mobile Network Alliance* and *LTE/SAE Trial Initiative*. The former is the alliance of major service providers who are mandated to complement and support the work within standardization bodies by providing a coherent view of what the operator community demands, whereas the latter is a global collaborative technology trial initiative focused on accelerating the availability of commercial and interoperable LTE mobile broadband systems to remove the hype from LTE and makes it more realistic.

Making LTE-Advanced system the favorite to win the 4G-battle and the most widely adopted 4G mobile communications, 3GPP has allowed individuals who are registered and eligible to be members of an Organizational Partners to participate in the technical work of that Organizational Partners if they are committed to support 3GPP and to contribute technically to the Technical Specification Groups within the 3GPP scope.

1.3.1. Structure of 3GPP

3GPP consists of a *Project Coordination Group* and *Technical Specification Groups.* The PCG is the highest decision making body which formally meets every 6 months to carry out the final adoption of 3GPP TSGs work items, to ratify election results and the resource committed to 3GPP. The TSGs accomplish the technical specification development work within 3GPP, and are responsible to prepare, approve and maintain the specifications contained in the project reference documentation (Partnership Project Description, Partnership Project Agreement, and Partnership Project Working Procedures), may organize their work in Working Groups and liaise other groups as appropriate, and finally report to the PCG. (3GPP Project Coordination Group 2012.)

1.4. Goal and Scope of the Thesis

The objective of this project is to compare the performances of MIMO channel equalization techniques such as MMSE, ZF and ZF-SIC equalizers in a Rayleigh multipath fading channel in 4G LTE-Advanced mobile networks and to recommend the best technique to service providers and vendors to settle worries before LTE-Advanced is commercially deployed in a span of a year. Simulation results validate the comparison techniques. Besides, MIMO channel capacities when there is channel information available at the transmitter and when the transmitter has no information about the channel, and access schemes of LTE system with emphasis on the effect of the peak amplitudes in the uplink transmission will be investigated.

1.5. Layout of the Thesis

With the technical background and introduction to LTE and its advanced version, the standard parameters and standardization phase of LTE system are presented in this first chapter; the subsequent chapters in this project are organized as follows:

Chapter 2: This chapter is the broadest chapter in which the downlink and uplink multiple access techniques of the 3GPP LTE system will be discussed in details. This chapter needs an immense attention as, for example, the proposal to use the already existing multiple access schemes like TDMA and OFDMA in the uplink transmission was intensely debated at the early stage of LTE development. The dire effect of high peak amplitudes arising from the several subcarriers with identical phase on the battery power of an end user led 3GPP to drop the proposal to use OFDMA in the uplink, and rather adopt SC-FDMA instead.

Chapter 3: In this chapter, the performance of different MIMO channel configurations is investigated. This includes the performance of the random MIMO channels when there is channel information available at the transmitter and when the transmitter does not have any access to get information about the channel.

Chapter 4: This chapter is the main part of the project in which techniques to equalize the effect of Rayleigh multipath MIMO channels on the transmission of symbols will be compared and simulated to propose the best techniques in the 4G LTE-Advanced networks. The commonly used techniques such as MMSE, ZF and SIC-ZF equalizers will be investigated.

Chapter 5: This is the last chapter where conclusions are drawn, and future works will be proposed for any enthusiasts who want to continue this work.

2. LTE MULTIPLE ACCESS BACKGROUND: DL OFDMA AND UL SC-FDMA

In LTE multiple access, OFDMA is supported in the downlink transmission while SC-FDMA is used in the uplink transmission.

In single carrier transmission, information is modulated only to one carrier, adjusting the phase and/or the amplitudes of the carrier, whereas in multiple carrier transmission different sub-carriers are used on which the data streams are divided to be sent over the same transmitter, with modulation around a different center frequency.

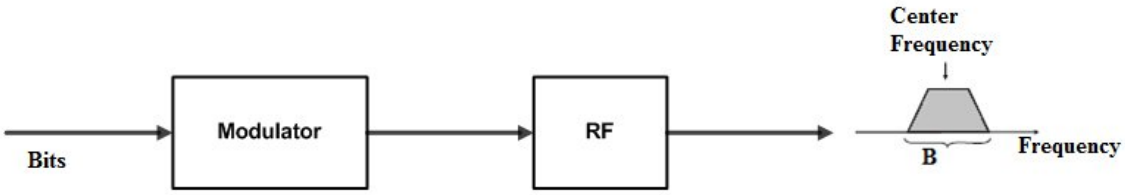

Figure 2.1. Single carrier transmission.

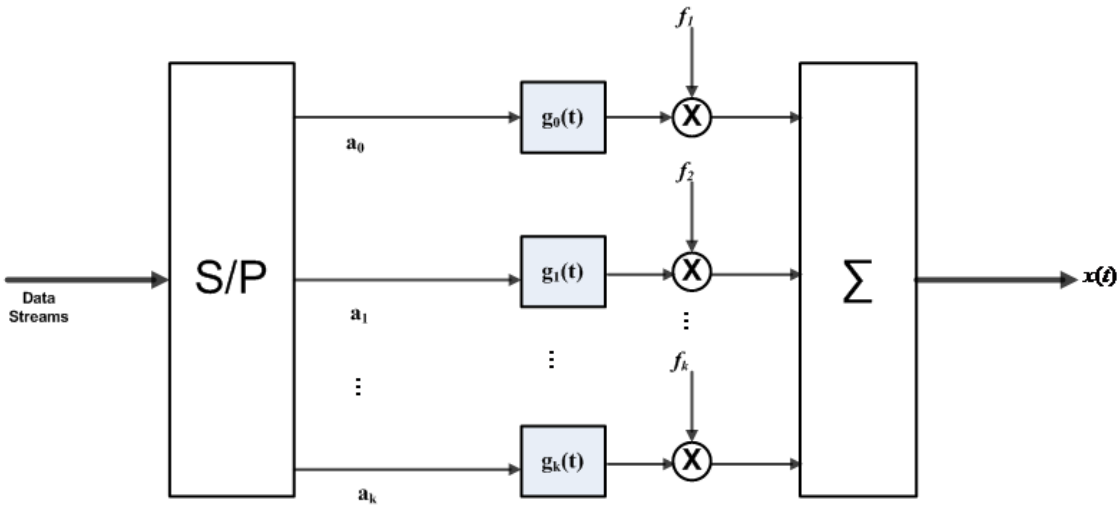

Figure 2.2. Block diagram of multiple carrier transmission.

2.1. Understanding OFDMA in LTE-Advanced

In 3G mobile networks, the use of OFDMA technology was not properly justified because there were some hindrances like the lack of definitive solution to uplink PAPR problem, the need for advanced antenna configuration and having radio resource management controlled in RNC. Once these problems were solved in later generations, the implementation of OFDMA system based on digital technology specifically on the use of FFT and the inverse operation IFFT has been widely employed. In OFDM transmission, a large number of closely spaced carriers that are modulated with low rate data are used. Because of the multitude of these carriers, the signals would normally be expected to interfere. But to avoid the spectrum inefficiency caused by the guard band requirements to spare sub-carriers interferences, orthogonality between different transmissions should be sought so that they do not interfere with each other. The orthogonality between these multiple

sinusoidal signals modulated by independent information is warranted by the frequency separation $\frac{1}{T}$, where *T* is the symbol period (Barry, Lee & Messerschmitt 2003: 215-230).

From figure 2.2 ,let the sinusoidal pulse signals in OFDM baseband transmission at k^{th} subcarrier be $g_k(t) = \frac{1}{T} e^{\frac{j2\pi kt}{T}} w(t) = \frac{1}{T} e^{j2\pi f_k t} w(t)$, *k*=0,1,…,*n*-1(*n* is the number of the subcarrier signals) and *w(t)=u(t)-u(t-T)* is a rectangular window over [0 *T*). For two sinusoidal signals having frequencies f_1 and f_2 of duration *T* and the phase difference between them over $[0\ 2\pi]$ to be orthogonal so that they can be distinguished at the receiver, the following equation should satisfy:

$$\int_0^T \cos(2\pi f_1 t + \theta)\cos(2\pi f_2 t)dt = 0 \ . \tag{2.1}$$

Using the following trigonometric identities will help us solve the above equation:

1. $\cos A \cos B = \frac{1}{2}[\cos(A+B) + \cos(A-B)]$,
2. $\sin A \cos B = \frac{1}{2}[\sin(A+B) + \sin(A-B)]$.

Then equation (2.1) will be solved as

$$\int_0^T \frac{1}{2}[\cos(2\pi(f_1+f_2)t+\theta) + \cos(2\pi(f_1-f_2)t+\theta)]dt = 0$$

$$\Rightarrow \cos\theta \int_0^T \cos 2\pi f_1 t \cos 2\pi f_2 t dt - \sin\theta \int_0^T \sin 2\pi f_1 t \cos 2\pi f_2 t dt = 0$$

$$\Rightarrow \cos\theta\int_0^T[\cos 2\pi(f_1+f_2)t+\cos 2\pi(f_1-f_2)t]dt-...$$
$$\sin\theta\int_0^T[\sin 2\pi(f_1+f_2)t+\sin 2\pi(f_1-f_2)t]dt=0$$
$$\Rightarrow \cos\theta[\frac{\sin 2\pi(f_1+f_2)T}{2\pi(f_1+f_2)}+\frac{\sin 2\pi(f_1-f_2)T}{2\pi(f_1-f_2)}]+...$$
$$\sin\theta[\frac{\cos 2\pi(f_1+f_2)T-1}{2\pi(f_1+f_2)}+\frac{\cos 2\pi(f_1-f_2)T-1}{2\pi(f_1-f_2)}]=0 \quad . \tag{2.2}$$

From trigonometry, note that $\sin(n\pi)=0$ and $\cos(n2\pi)=1$, where n is an integer. Let us assume $(f_1+f_2)\ T$ to be an integer. Then equation (2.2) will be simplified as

$$\cos\theta[\frac{\sin 2\pi(f_1-f_2)T}{2\pi(f_1-f_2)}]+\sin\theta[\frac{\cos 2\pi(f_1-f_2)T-1}{2\pi(f_1-f_2)}]=0 \ . \tag{2.3}$$

When θ is a random variable between 0 and 2π , equation (2.3) can hold if and only if $\sin 2\pi(f_1-f_2)T=0$ and $\cos 2\pi(f_1-f_2)T=1$. To satisfy this requirement,

$$2\pi(f_1-f_2)T=n2\pi \tag{2.4}$$
$$\Rightarrow f_1-f_2=\frac{n}{T}.$$

Since the minimum value of n is 1, then the minimum frequency separation will be $f_1-f_2=\frac{1}{T}$. But when $\theta=0$, equation (2.3) will be simplified as

$$\frac{\sin 2\pi(f_1-f_2)T}{2\pi(f_1-f_2)}=0$$
$$\Rightarrow \sin 2\pi(f_1-f_2)T=0 \ . \tag{2.5}$$

For equation (2.5) to satisfy the requirement, the following equation holds:

$$2\pi(f_1 - f_2)T = n\pi \tag{2.6}$$
$$\Rightarrow f_1 - f_2 = \frac{n}{2T}.$$

Of course since the minimum value of n is 1, the minimum frequency separation will be given as $f_1 - f_2 = \frac{1}{2T}$.

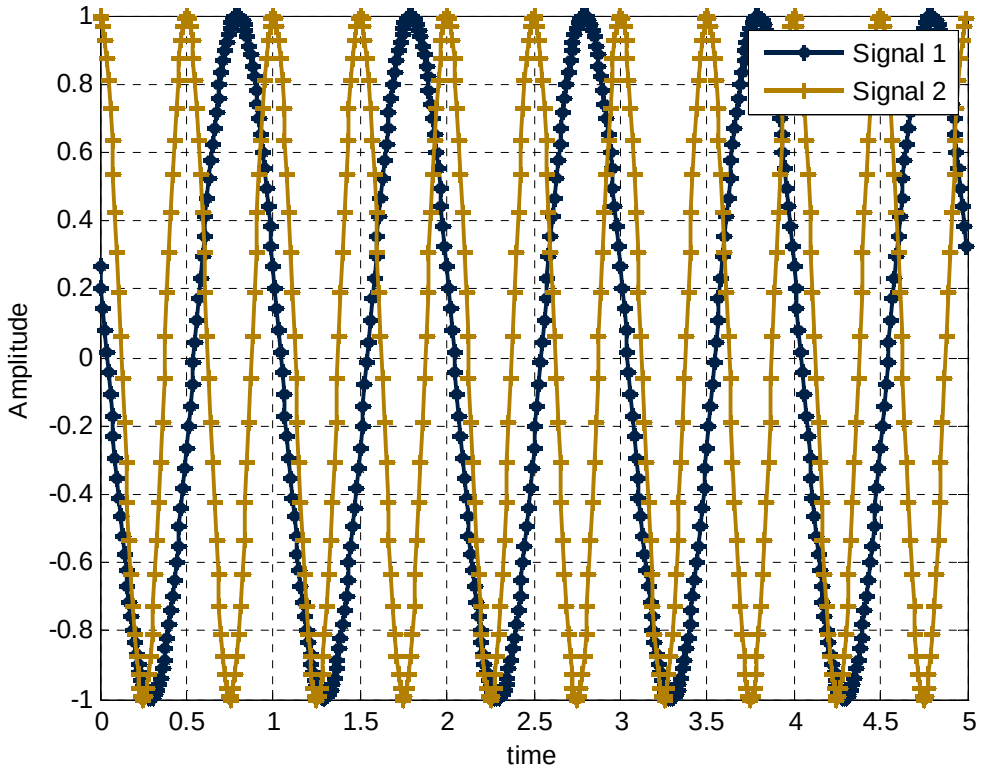

Figure 2.3. Two sinusoidal signals with minimum frequency separation $\frac{1}{T}$ for random phase.

The plot shows that the minimum frequency separation between the signals is $\frac{1}{T}$ for them to be orthogonal when the phase between them is not known.

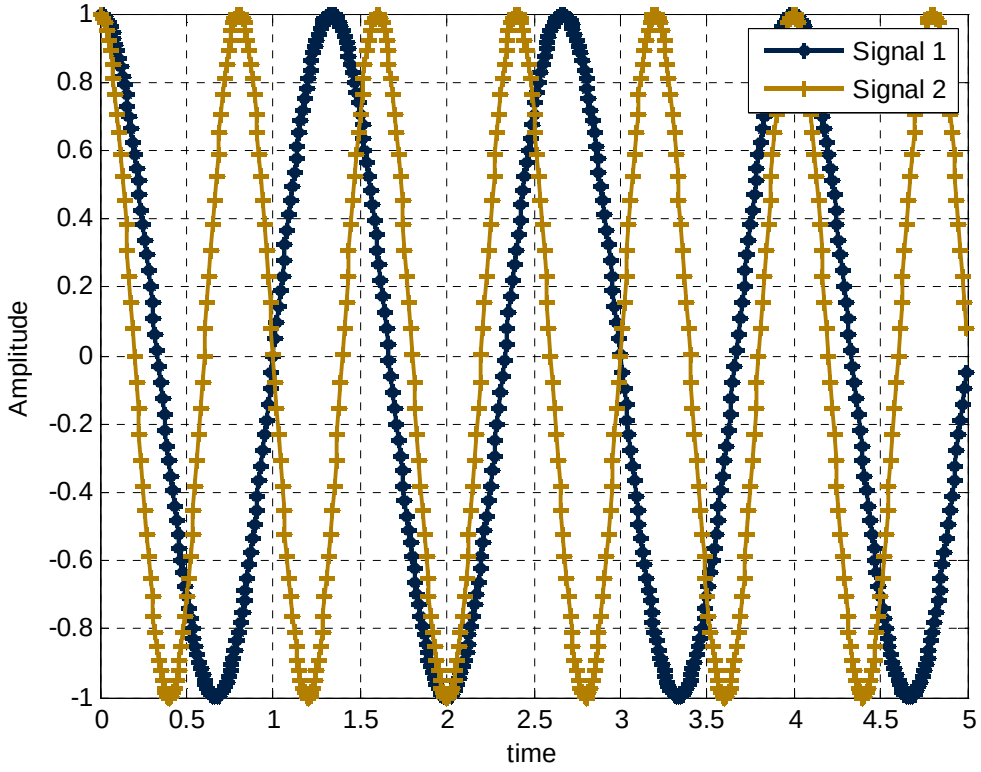

Figure 2.4. Two sinusoidal signals with minimum frequency separation $\frac{1}{2T}$ for zero phase.

The plot shows that the minimum frequency separation between the two sinusoidal signals is $\frac{1}{2T}$ for them to be orthogonal when the phase is zero.

According to Holma et al. (2009:69), the overall motivations to use OFDMA in downlink multiple access of LTE system are:

- Good performance in frequency selective fading channels;
- Low complexity of baseband receiver;
- Good spectral properties and handling of multiple bandwidths ;
- Link adaptation and frequency domain scheduling ; and
- Compatibility with advanced receiver and antenna technologies.

Whereas the challenges of OFDMA in broadband wireless systems:

- Interference between neighboring sub-carriers. This issue has been solved in LTE system design by setting sub-carrier spacing to be 15 kHz regardless of the total transmission bandwidth; and
- In the uplink multiple access, the high PAR has hindered the performance of transmitter, because the linear amplifiers have low power conversion efficiency. But in LTE, SC-FDMA with better power amplifier efficiency has to come to its rescue.

2.1.1. OFDMA Implementation by FFT/IFFT

The transmitter of an OFDMA system synthesizes the transmit signal from a serial-to-parallel converted data source using the IFFT block, followed by adding the cyclic prefix (the copy of the end of symbol inserted at the beginning) longer than the channel impulse response (spread delay) to avoid ISI interference. Whereas at the receiver side, the analysis of the signal is implemented by the FFT block, in which the size of FFT for LTE system must be chosen to be significantly larger than the number of modulated carriers to ensure that the edge of effects are neglectable at half the sampling frequency and to ensure the shape of the reconstruction filter of the DAC does not affect the significant part of the spectrum (Schulze & Lüders 2005: 162-165). At the same time, the baseband signal will be analog-to-digital converted. Then, for each block of N_{FFT} samples, an FFT length is performed, of which k useful spectral coefficients will be used, and with the remaining N_{FFT}

-*k* spectral coefficients outside the transmission band are set to zero. Thus for LTE, the practically implemented size of FFT is 1024 even if only 600 outputs are used.

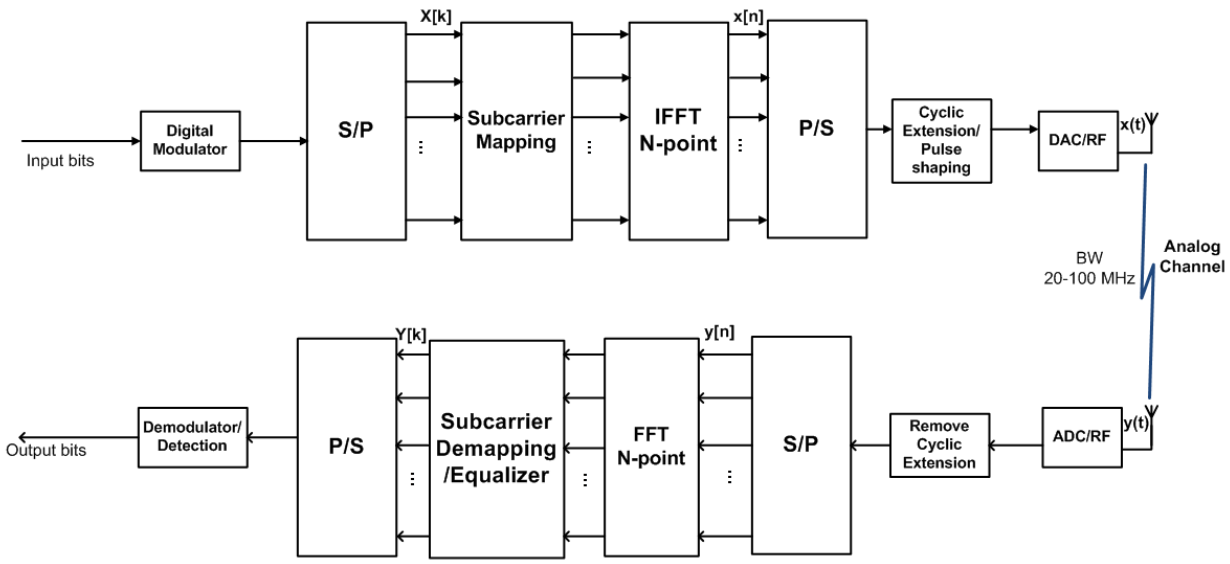

Figure 2.5. Block diagram of OFDMA transmitter and receiver with frequency domain signal generation.

2.1.2. Distribution of Output Signals for IFFT in the OFDMA Systems

From figure 2.5, the discrete-time signal after IFFT transmitter can be given as

$$x[n] = \frac{1}{N}\sum_{k=0}^{N-1} X[k] e^{\frac{j2\pi kn}{N}}, \tag{2.7}$$

where $X[k]$ is a sequence of PSK or QAM modulated data symbols in frequency domain. This equation shows that adding the N different time-domain signals $\{e^{\frac{j2\pi kn}{N}}\}$, each of

which corresponds to different orthogonal subcarriers, the k^{th} signal modulated with data symbol $X[k]$, generates the discrete time signal $\{x[n]\}$.

The input signals of N-point IFFT have independently and finite magnitudes which are uniformly distributed for QPSK and QAM so that the imaginary and real parts of time-domain complex OFDMA signal $x(t)$ after IFFT at the transmitter have Gaussian distributions for a large number of subcarriers by the CLT ,and the amplitude $|x(t)|$ of the signal will then follow a Rayleigh distribution.

If the normalized average power $E[|x(t)|^2]$ of $x(t)$ is assumed to be unity, then the magnitudes $\{|x[n]|\}$ of the complex samples $\{|x[nT_s/N]|\}_{n=0}^{N-1}$ are independent and identically distributed Rayleigh random variables with the following probability density function:

$$f_{|x[n]|}(x) = \frac{x}{\sigma^2} e^{\frac{-x^2}{2\sigma^2}} = 2xe^{-x^2}, \tag{2.8}$$

where $E(|x[n]|^2) = 1 = 2\sigma^2$, and $n = 0,1,\cdots,N-1$. The CDF of $X_{\max} = \max|x[n]|_{n=0}^{N-1}$ is given as

$$\begin{aligned} F_{X_{\max}}(x) &= P(X_{\max} < x) \\ &= P(X_0 < x).P(X_1 < x)...P(X_{N-1} < x) \\ &= (1 - e^{-x^2})^N, \end{aligned} \tag{2.9}$$

where $P(X_n < x) = \int_0^x f_{X_n}(x)dx$.

In order to find the probability that $X_{\max}$ exceeds x, CCDF should be evaluated as follows, according to Ross (2010: 301-302):

$$\begin{aligned}\widetilde{F}_{X_{\max}}(x) &= P(X_{\max} > x) \\ &= 1 - P(X_{\max} \le x) \\ &= 1 - F_{X_{\max}}(x) \\ &= 1 - (1 - e^{-x^2})^N . \end{aligned} \tag{2.10}$$

Obviously, the main purpose of oversampling signals is to approximate the continuous-time signal because a sampled signal does not necessarily contain the maximum point of the original continuous-time signal. Thus, the CDF of oversampled signals will be approximated as

$$F_X(x) = (1 - e^{-x^2})^{\alpha N}, \tag{2.11}$$

where $\alpha = 2.8$ for sufficiently large N.

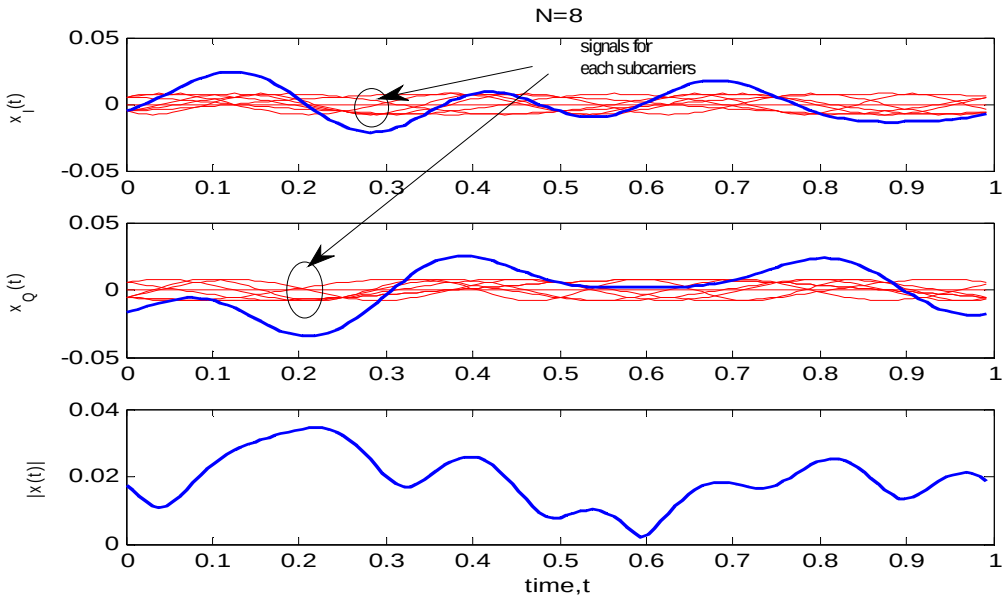

Figure 2.6a. Time-domain OFDMA baseband signals using QPSK.

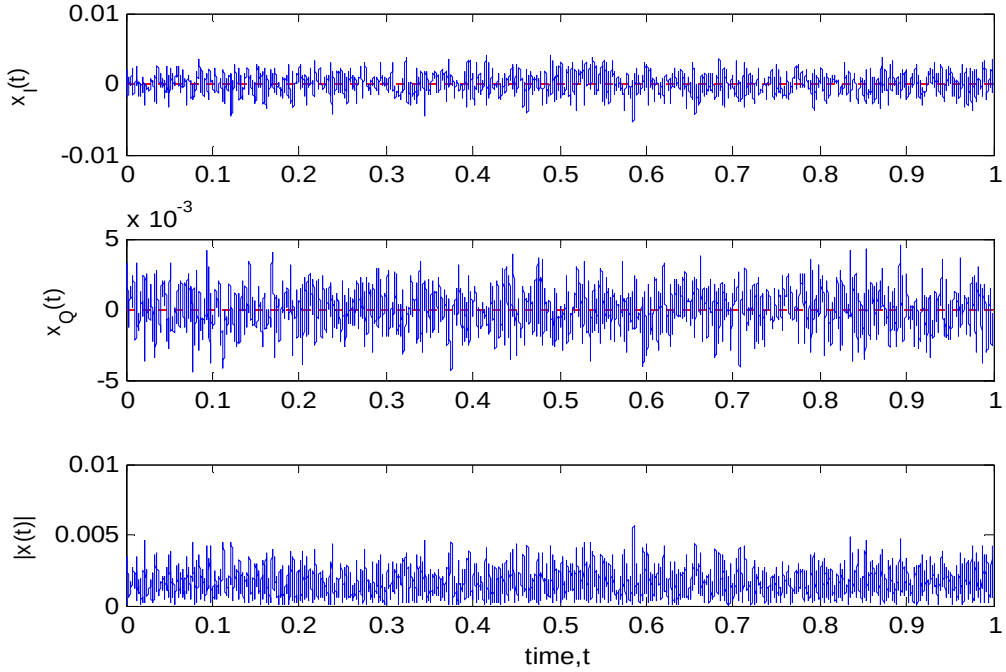

Figure 2.6b. Time-domain OFDMA baseband signals using QPSK (*N*=1024).

Figures show the individual time-domain QPSK modulated subcarrier signals $X[k]e^{\frac{j2\pi kn}{N}}$ for IFFT N=8, and 1024 respectively, and the sum of the continuous-time version $x(t)$ of $x[n]$. The simulation results confirm that the real and imaginary components of $x[n]$ have a Gaussian distribution while the distribution of $|x[n]|$ will follow a Rayleigh distribution. It is also worth noting that the effect of PAPR becomes significant as the value of N increases but the probability that it happens will decrease.

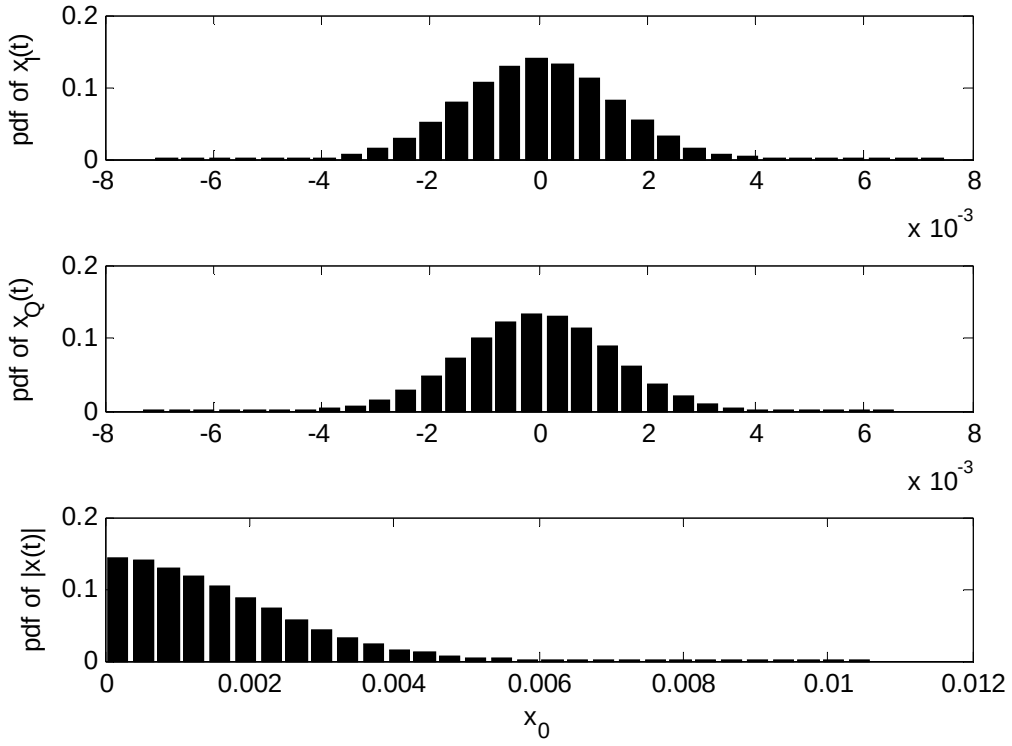

Figure 2.7. Magnitude distribution of OFDMA signal using QPSK (N=1024).

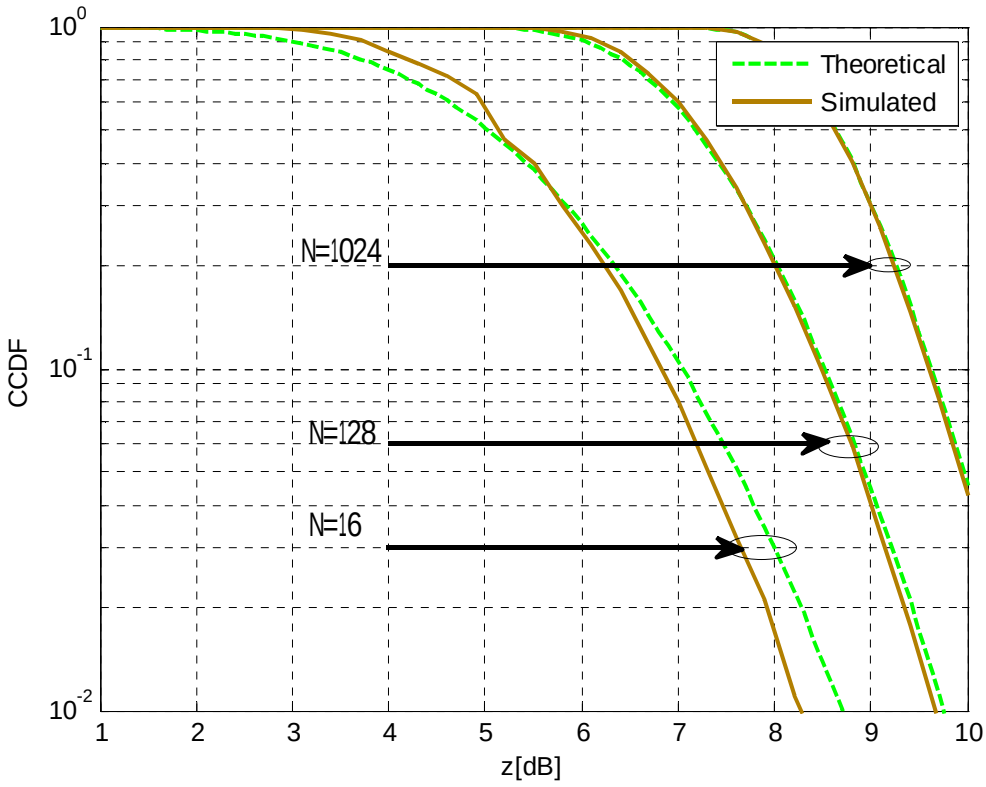

Figure 2.8. CCDFs of OFDMA signals with different *N*-FFT values using 64-QAM modulation.

The plot shows that the simulated results are overlapping with the ideal ones as the value of number of FFT increases. This implies that equations (2.9) and (2.11) exactly match only when *N* is sufficiently large.

2.1.3. Modulation and Demodulation of OFDMA Signals

In section 2.1, an OFDMA pulse signal in baseband transmission at k^{th} subcarrier is given to be $g_k(t) = \frac{1}{T} e^{j2\pi f_k t}$, for $0 < t \le T$. Then, from figure 2.5, the passband and the complex transmit baseband signals in continuous-time domain can be expressed, respectively as

$$x(t) = \Re\{\sum_{k=0}^{N-1} X[k] \times g_k(t)\} \ ,$$

$$x_b(t) = \sum_{k=0}^{N-1} X[k] g_k(t) \ . \tag{2.12}$$

If the received baseband OFDMA symbol is given as

$$y(t) = \sum_{k=0}^{N-1} X[k] e^{j2\pi f_k t}, \text{ for } T < t \le T + nT_s \ , \tag{2.13}$$

where $T = NT_s$, is the duration of the system transmission time for N symbols after S/P conversion, and T_s is the duration of the original symbol $X[k]$.

Without the effects of channel and noise, the transmitted symbol $X[k]$ can be recovered by the orthogonality among the subcarriers as follows:

$$\begin{aligned} Y[k] &= \frac{1}{T} \int_{-\infty}^{\infty} y(t) e^{-j2\pi f_k t} dt \\ &= \frac{1}{T} \int_{-\infty}^{\infty} (\sum_{i=0}^{N-1} X[i] e^{j2\pi f_i t}) e^{-j2\pi f_k t} dt \\ &= \sum_{i=0}^{N-1} X[i] \{\frac{1}{T} \int_0^T e^{j2\pi (f_i - f_k) t}\} dt \ = X[k]. \end{aligned} \tag{2.14}$$

Using the discrete-time representation, the same result as equation (2.14) will be obtained after the demodulation process of the transmitted symbol. The discrete-time domain form of the received signal is represented as

$$y[n] = \frac{1}{N}\sum_{k=0}^{N-1} X[k] e^{\frac{j2\pi kn}{N}} \quad . \tag{2.15}$$

Thus, the frequency-domain representation of the received signal after *N*-point FFT receiver is evaluated as

$$Y[k] = \sum_{n=0}^{N-1} y[n] e^{-j2\pi kn/N} \tag{2.16}$$

$$= \sum_{n=0}^{N-1} \{\frac{1}{N}\sum_{i=0}^{N-1} X[i] e^{j2\pi in/N}\} e^{-j2\pi kn/N}$$

$$= \frac{1}{N}\sum_{n=0}^{N-1}\sum_{i=0}^{N-1} X[i] e^{j2\pi(i-k)n/N} = X[k]. \tag{2.17}$$

But in the presence of multipath path channel and AWGN effects, the convolved received signal is given as

$$y(t) = x(t) * h(t) + z(t) = \int_0^{\infty} h(\tau)x(t-\tau)dt + z(t)\,, \tag{2.18}$$

where $h(t)$ is the impulse response of the channel and $z(t)$ is the AWGN process. Taking the samples of equation (2.18) at $nT_s = nT/N$, the discrete-time representation of the received signal will be given as

$$y[n] = x[n] * h[n] + z[n] = \sum_{m=0}^{\infty} h[m]x[n-m] + z[n], \tag{2.19}$$

where $y[n] = y[nT_s]$, $x[n] = x[nT_s]$, $h[n] = h[nT_s]$, and $z[n] = z[nT_s]$. Then after the receiver N-point FFT, the received symbol in frequency-domain will be evaluated as follows:

$$\begin{aligned} Y[k] &= \sum_{n=0}^{N-1} y[n] e^{-j2\pi kn/N} \\ &= \sum_{n=0}^{N-1} (\sum_{m=0}^{\infty} h[m]x[n-m] + z[n]) e^{-j2\pi kn/N} \\ &= \sum_{n=0}^{N-1} \{\sum_{m=0}^{\infty} h[m](\frac{1}{N}\sum_{i=0}^{N-1} X[i] e^{j2\pi i(n-m)/N}) + z[n]\} e^{-j2\pi kn/N} \\ &= \frac{1}{N}\sum_{n=0}^{N-1} \{(\sum_{m=0}^{\infty} h[m] e^{-j2\pi im/N}) X[i] \sum_{n=0}^{\infty} e^{-j2\pi(k-i)n/N}\} e^{-j2\pi kn/N} + Z[k] \\ &= X[k]H[k] + Z[k], \end{aligned} \tag{2.20}$$

where $H[k]$ and $Z[k]$ are the k^{th} subcarrier frequency-domain components of the channel frequency response and the noise frequency, respectively.

2.2. Understanding SC-FDMA

It has been discussed in the previous section 2.1 that in OFDMA transmission, the large number of subcarriers with different frequencies will amount to the Gaussian distribution of transmit signals with different peak amplitude values in time-domain which has a high PAPR that can cause some challenges to the amplifier design. Allowing the peaks to distort is catastrophic because this causes the spectral regrowth in the adjacent channels, the uplink range to be shorter and the battery energy to be consumed faster due to higher amplifier

power consumption. Modifying the amplifier to avoid the distortion obviously requires increases in cost, size and power consumption.

Making the OFDMA transmission worse, minimizing the lost efficiency caused by inserting the cyclic extension in the tight spacing of subcarriers demands very long symbols (which means very closely spaced subcarriers). This will not only increase the processing time but also force the subcarriers to lose orthogonality due to frequency errors, which will consequently impair performance.

These two major problems of OFDMA led 3GPP to adopt a different modulation technique in LTE uplink – SC-FDMA which is an uplink multiple access scheme in LTE system that utilizes single carrier modulation, DFT-spread orthogonal frequency multiplexing, and frequency domain equalization.

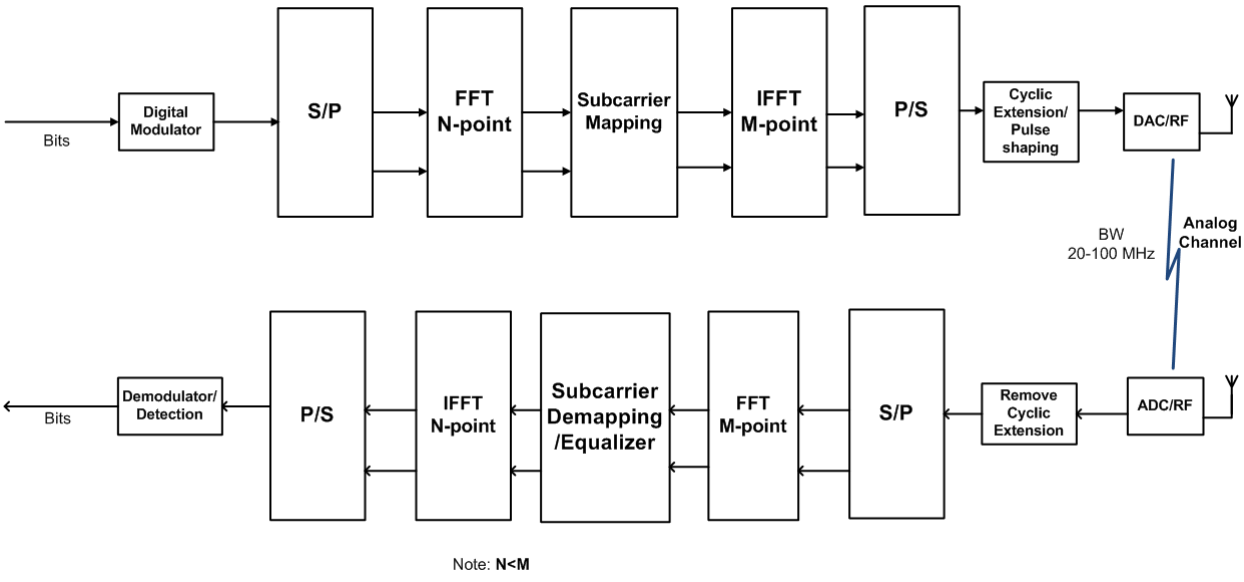

Figure 2.9. Block diagram of SC-FDMA transmitter and receiver with frequency domain signal generation.

2.2.1. Capacity Evaluation Results in the Uplink

By using simple analytical models, it is possible to provide a channel capacity performance comparison of orthogonal uplink multiple access techniques, such as TDMA, OFDMA and SC-FDMA and a non-orthogonal uplink multiple access WCDMA.

In a WCDMA system, multiple users transmitting at the same time interfere with each other due to the asynchronous nature of the received uplink transmission. The uplink capacity limit of a WCDMA modulation is given as

$$C_{WCDMA} = k\log_2(1+\frac{p}{(1+f)kp+(\varpi-1)p+N_0})$$

$$= k\log_2(1+\frac{SNR}{(1+f)kSNR+(\varpi-1)SNR+1}) \text{ bps/Hz,} \quad (2.21)$$

where k is the number of users at a time, p is the received power to a user, f is the ratio between other-cell and own-cell signal, ϖ is the fraction of the own-user signal considered as interference, and N_0 is the background noise.

In a TDMA system, a single user transmits at a given time slot so that the total system resource is shared among multiple users accessing the channel link on time slot basis. Thus, the uplink capacity limit of a TDMA system (k=1) is given as

$$C_{TDMA} = k\log_2(1+\frac{p}{(1+f)kp+(\varpi-1)p+N_0})$$

$$= \log_2(1+\frac{p}{(\varpi+f)p+N_0})$$

$$= \log_2(1+\frac{SNR}{(\varpi+f)SNR+1}) \text{ bps/Hz.} \quad (2.22)$$

We have discussed in the previous sections that in an OFDMA system, multiple users on orthogonal subcarriers share the resources by allocating to a user only a fraction of the total bandwidth. Therefore, the uplink capacity limit for an OFDMA system is given as

$$\begin{aligned} C_{OFDMA} &= \sum_{i=1}^{k} B_i \log_2(1+\frac{p}{fp+B_i N_0}) \\ &= \sum_{i=1}^{k} \frac{1}{k} \log_2(1+\frac{p}{fp+\frac{N_0}{k}}) \\ &= \log_2(1+\frac{kp}{kfp+N_0}) \\ &= (\frac{T_s}{T_s+T_{cp}}) \log_2(1+\frac{kp}{kfp+N_0}) \\ &= (\frac{T_s}{T_s+T_{cp}}) \log_2(1+\frac{kSNR}{kfSNR+1}) \text{ bps/Hz,} \end{aligned} \tag{2.23}$$

where T_s is the symbol duration ,and T_{cp} is the cyclic prefix duration.

Like OFDMA, there is no intra-cell interference in SC-FDMA uplink transmission due to orthogonal subcarriers. Hence, the uplink capacity limit for SC-FDMA modulation technique is written as

$$\begin{aligned} C_{SC-FDMA} &= (\frac{T_s}{T_s+T_{cp}}) \log_2(1+\frac{kp}{kfp+N_0} \times \frac{1}{10^{(L_{SC}/10)}}) \\ &= (\frac{T_s}{T_s+T_{cp}}) \log_2(1+\frac{kSNR}{kfSNR+1} \times \frac{1}{10^{(L_{SC}/10)}}) \text{ bps/Hz,} \end{aligned} \tag{2.24}$$

where L_{SC} is the SC-FDMA loss in dBs relative to OFDMA.

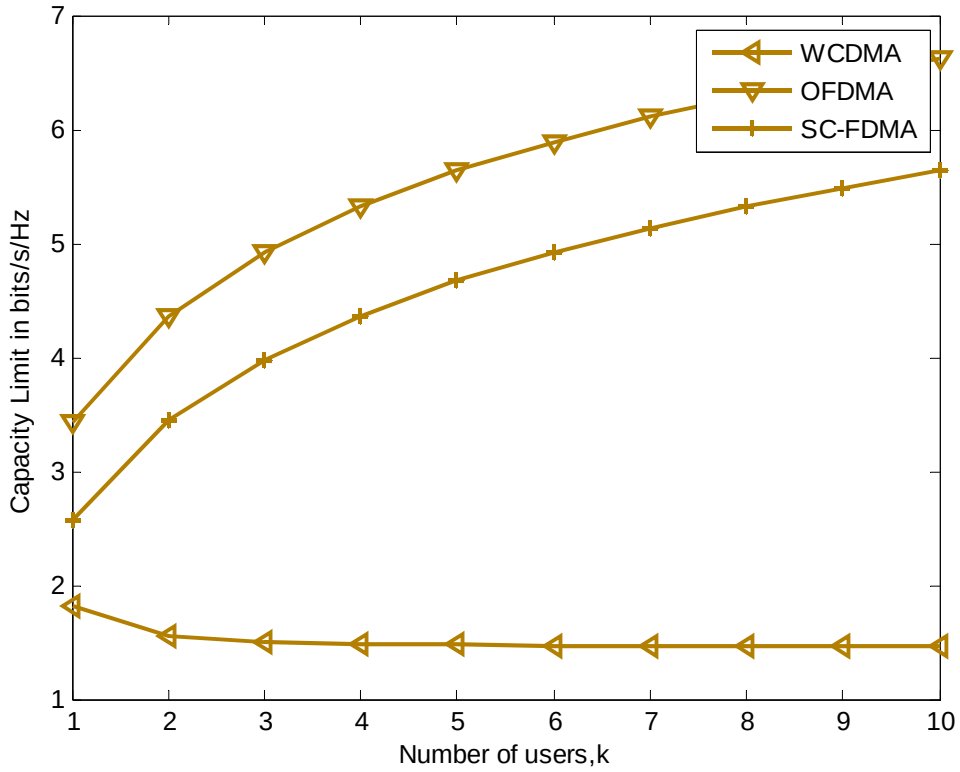

Figure 2.10a. Uplink capacity limits for WCDMA, OFDMA and SC-FDMA for single cell scenario (f=0, ϖ=0.3, $T_s = 10ms$, $T_{cp} = 66.7\mu s$, $L_{SC} = 3dB$ and SNR=10 dB).

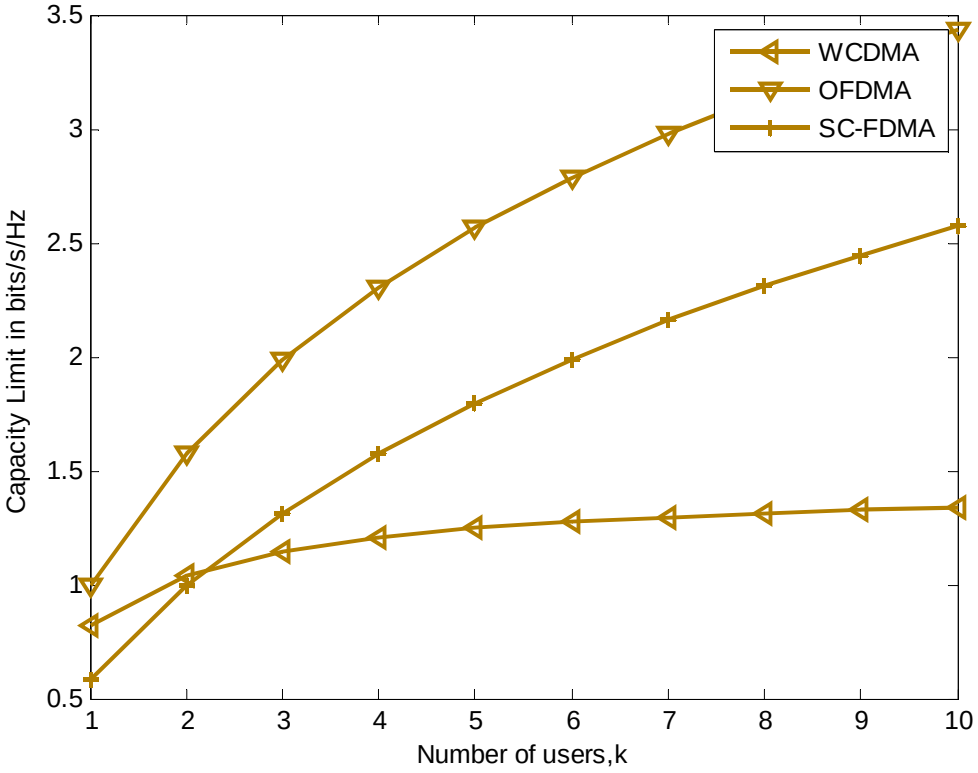

Figure 2.10b. Uplink capacity limits for WCDMA, OFDMA and SC-FDMA for single cell scenario (*SNR*=0 dB).

The simulation results show that as the number of the users closer to the base station (*SNR*=10 dB) simultaneously accessing the system increases, the performance of the orthogonal multiple access schemes improves over that of the non-orthogonal multiple access which drops steadily. This is because for a high *SNR* user, non-orthogonal multiple access suffers from inter-user (intra-cell) interference while orthogonal multiple access techniques benefit by eliminating the intra-cell interference. This is one of the reasons which led 3GPP to rule out the adoption of TDMA and WCDMA approaches at a very early stage of LTE system design. On the other hand, even if intra-cell interference is still eliminated, orthogonal multiple access schemes provide only a small improvement for a low *SNR* user due to an inter-cell interference and the background noise. It is also worth

noting that WCDMA outperforms SC-FDMA for a weak user at a small number of users. Moreover, the benefit of OFDMA and SC-FDMA is that multiple users can simultaneously transmit providing larger power transmitted in the system.

2.2.2. Generation of Transmit Symbols in SC-FDMA Modulation

In uplink multiple channel access, each mobile terminal uses a subset of subcarriers with the rest unused ones filled with zeros. The assigning of subcarriers among the corresponding users is usually done by DFDMA and LFDMA schemes.

Let us look at how to generate SC-FDMA transmit symbols. FFT precoding of the data sequence and then mapping of the FFT-precoded data sequence to uniformly spaced subcarriers at the input of IFFT is worth considering to mathematically analyzing it. The uniform spacing is determined by the repetition/spreading factor Q of the data sequence.

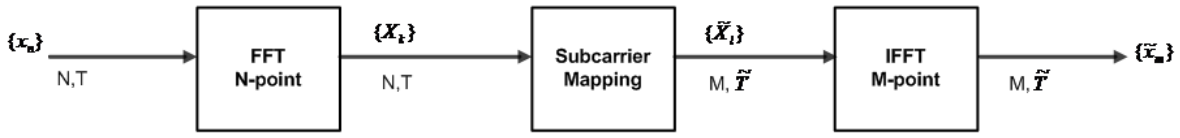

Figure 2.11. Generation of SC-FDMA transmit symbols.

In the above figure, DFDMA distributes N FFT outputs over the entire band of total M subcarriers with zeros filled in M-N unused subcarriers, whereas LFDMA allocates FFT outputs to N consecutive subcarriers in M subcarriers.

Details of the figure:

Let $\{x_n : n = 0,1,...,N-1\}$ be the data symbols to be modulated.

Then, $\{X_k : k = 0,1,...,N-1\}$ are the frequency domain samples after FFT of x_n,

$\{\widetilde{X}_l : l = 0,1,...,M-1\}$ are the frequency domain after subcarrier mapping ,

and $\{\widetilde{x}_m : m = 0,1,...,M-1\}$ are the time domain symbols after IFFT of $\widetilde{X}_l$.

It is seen from the diagram that there are *M* subcarriers, among which *N* subcarriers are occupied by the input data. In time domain, the input data has symbol duration *T*, and the symbol duration is compressed to $\widetilde{T} = (\frac{N}{M})T$ after going through SC-FDMA modulation. The mapping of FFT-precoded data sequence to contiguous subcarriers results in a localized transmission in frequency domain. This is represented as

$$X_k = \sum_{n=0}^{N-1} x_n e^{\frac{-j2\pi kn}{N}} . \tag{2.25}$$

To derive the time domain symbols of FDMA $\{x_m\}$ which are obtained by taking IFFT of $\{\widetilde{X}_l\}$, we need to define $m = N.q + n$, where $0 \le q \le Q-1$, $0 \le n \le N-1$ and *M=NQ*. For distributed FDMA, the input frequency samples to IFFT after subcarrier mapping can be given as

$$\widetilde{X}_l = \begin{cases} X_{l/Q}, & for\ l = Q.k, 0 \le k \le N-1 \\ 0, & otherwise. \end{cases} \tag{2.26}$$

Then, the time-domain samples at output of IFFT are given as

$$\begin{aligned}\tilde{x}_m &= \frac{1}{M}\sum_{l=0}^{M-1}\tilde{X}_l e^{\frac{j2\pi ml}{M}} = \frac{1}{NQ}\sum_{k=0}^{N-1}x_k e^{\frac{j2\pi mk}{N}} \\ &= \frac{1}{NQ}\sum_{k=0}^{N-1}x_k e^{\frac{j2\pi(Nq+n)k}{N}} \\ &= \frac{1}{Q}\left(\frac{1}{N}\sum_{k=0}^{N-1}x_k e^{\frac{j2\pi nk}{N}}\right) \\ &= \frac{1}{Q}x_n .\end{aligned} \tag{2.27}$$

This shows that the resulting time symbols at the output of size *M* IFFT are simply the repetitions of the original time-domain symbols at the input of size *N* FFT. Therefore, the PAPR of the signal is same as in the case of conventional single carrier signal.

For localized FDMA, the frequency samples after subcarrier mapping can be given as

$$\tilde{X}_l = \begin{cases} X_l, & 0 \le l \le N-1 \\ 0, & N \le l \le M-1. \end{cases} \tag{2.28}$$

Then, the time-domain samples at output of IFFT are given as

$$\begin{aligned}\tilde{x}_m &= \frac{1}{M}\sum_{l=0}^{M-1}\tilde{X}_l e^{\frac{j2\pi ml}{M}} \\ &= \frac{1}{NQ}\sum_{l=0}^{N-1}X_l e^{\frac{j2\pi(Qn+q)l}{NQ}} .\end{aligned} \tag{2.29}$$

If q=0, equation (2.29) will be simplified as

$$\begin{aligned}\tilde{x}_m &= \frac{1}{NQ}\sum_{l=0}^{N-1} X_l e^{\frac{j2\pi Qnl}{NQ}} \\ &= \frac{1}{Q}\left(\frac{1}{N}\sum_{l=0}^{N-1} X_l e^{\frac{j2\pi nl}{N}}\right) \\ &= \frac{1}{Q} x_n \ . \end{aligned} \tag{2.30}$$

It can be seen that every Q^{th} time-domain sample at the output size M IFFT is the same as the time-domain sample at the input of size N FFT.

If $q \neq 0$, since $X_l = \sum_{p=0}^{N-1} x_p e^{\frac{-j2\pi pl}{N}}$, then equation (2.29) can be expressed as

$$\begin{aligned}\tilde{x}_m &= \frac{1}{Q}\left(\frac{1}{N}\sum_{l=0}^{N-1} X_l e^{\frac{j2\pi (Qn+q)l}{NQ}}\right) \\ &= \frac{1}{Q}\left(\frac{1}{N}\sum_{l=0}^{N-1}\sum_{p=0}^{N-1} e^{\frac{-j2\pi pl}{N}} e^{\frac{j2\pi (Qn+q)l}{NQ}}\right) \\ &= \frac{1}{Q}\left(1-e^{\frac{j2\pi p}{Q}}\right)\frac{1}{N}\sum_{p=0}^{N-1}\frac{x_p}{1-e^{j2\pi\left(\frac{n-p}{N}+\frac{p}{QN}\right)}} \ . \end{aligned} \tag{2.31}$$

As can be seen from equation (2.31), the time-domain sample at the output of size M IFFT is the sum of time-domain samples at the input of size N FFT with different complex-weighting which would increase the PAPR.

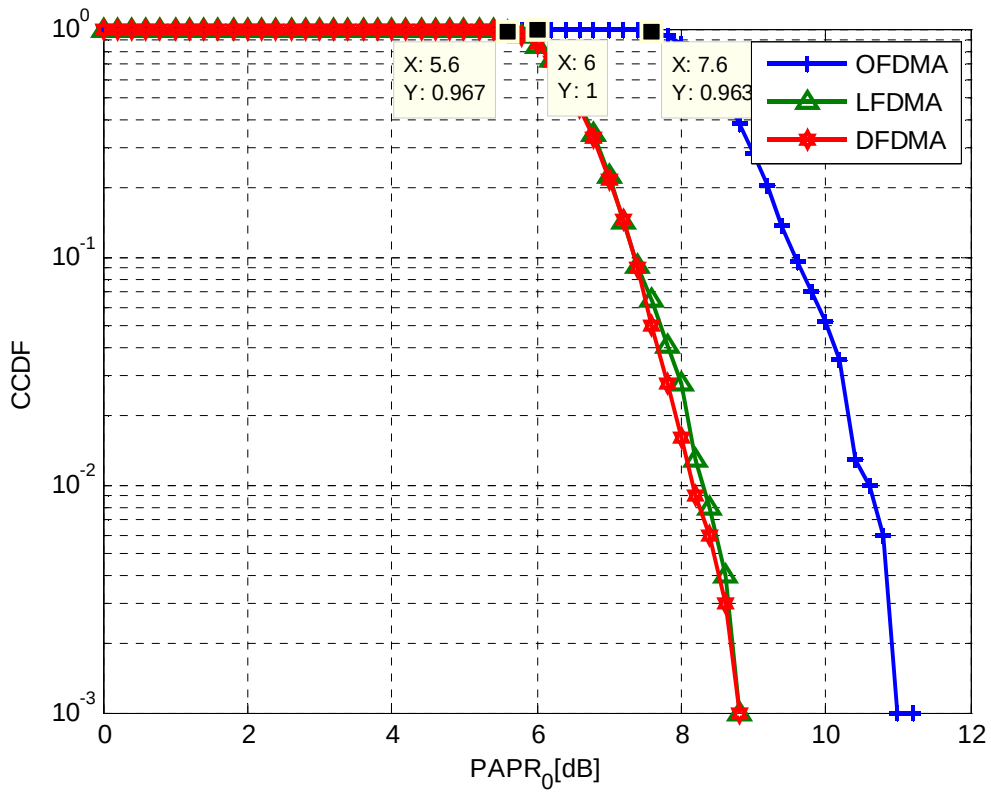

Figure 2.12. PAPR performances for DFDMA, LFDMA and OFDMA using 16-QAM.

The plot compares the CCDF of PAPR when DFT-spreading technique is applied to DFDMA, LFDMA and OFDMA systems using the total number of subcarriers=1024,the FFT input data block size =256,transmission bandwidth B=20 MHz, oversampling factor L= 8, and spreading factor Q=1024/256=4 as parameters. Here, CCDF of PAPR is the probability that PAPR is higher than certain value $PAPR_0$, that is, $\Pr(PAPR > PAPR_0)$. The simulation result shows the PAPR values at CCDF of 1% with DFDMA, LFDMA and OFDMA are 5.6 dB, 6 dB and 7.6 dB, respectively. This implies that DFDMA has lower PAPR than that of OFDMA without DFT-spreading by 2 dB, while PAPR of LFDMA is lower than that of OFDMA by 1.6 dB but higher than that of DFDMA by 0.4 dB.

2.3. Introduction to PAPR

Due to the transmit power limitations, it takes longer to transmit a given amount of data in the uplink multiple access transmission, which consequently adds delays in the system and a signaling overhead. This would be solved by increasing the uplink power amplifier size which would come at the expense of increased cost and end user battery consumption. The backoff required due to PAPR of the transmit signal will lead to transmit power inefficiency.

To analyze the PAPR of the SC-FDMA signal for each subcarrier mapping mode, the complex passband transmit signal $x(t)$ for a block of data is given as

$$x(t) = e^{j2\pi f_c t} \sum_{m=0}^{M-1} \tilde{x}_m(t) r(t - m\tilde{T}) \ , \tag{2.32}$$

where f_c is the carrier frequency of the system and *r(t)* is the baseband pulse. The PAPR of passband transmit signal *x(t)* is expressed as

$$PAPR = \frac{\max|x(t)|^2}{E[|x(t)|^2]} = \frac{\max|x(t)|^2}{\frac{1}{M\tilde{T}} \int_0^{M\tilde{T}} |x(t)|^2 dt} \ . \tag{2.33}$$

Without using pulse shaping but using rectangular pulse shaping, the symbol rate sampling will give the same PAPR as the continuous case since the SC-FDMA signal is modulated over a single carrier. Thus, the PAPR with the symbol rate sampling can be expressed as

$$PAPR = \frac{\max|\tilde{x}_m|^2}{\frac{1}{M}\sum_{m=0}^{M-1}|\tilde{x}_m|^2}. \quad (2.34)$$

2.3.1. PAPR of QAM Modulations

Higher power can be transmitted in the uplink for the same power amplifier size by reducing the uplink signal peakiness. This can be done by advanced low PAPR modulations and spectrum shaping.

Unlike WCDMA uplink which suffers from higher order modulations intra-cell interference due to the non-orthogonal multiple subcarriers accessing the channel simultaneously , LTE system uses higher order modulations to achieve the target higher data rates up to 500 Mb/s in pedestrian environment ,based on SC-FDMA orthogonal uplink access which avoids the intra-cell interference. Unfortunately, this would cause higher PAPR and larger power amplifier back-offs on the uplink reducing the total available transmission power. Of course, the higher data rates in the uplink can be achieved by using MIMO spatial multiplexing techniques. In this section, the PARP for QPSK, 16-QAM and 64-QAM modulations will be compared.

In QPSK modulation, assuming a unit average power, the real and imaginary parts take amplitude values A and $-A$ where A is given as

$$\frac{4(A^2 + A^2)}{4} = 1$$
$$\therefore A = \frac{1}{\sqrt{2}} \quad . \quad (2.35)$$

Since all the constellation points have the same power, PAPR can be evaluated as

$$PAPR_{QPSK} = \frac{(A^2 + A^2)}{1} = 2A^2 = 1 = 0dB \ . \tag{2.36}$$

Again assuming a unit average power, the real and imaginary parts of 16-QAM take amplitude values of *A, 3A, A* and *-3A*, where *A* is given as

$$\frac{4(A^2 + A^2 + A^2 + 9A^2 + A^2 + 9A^2 + 9A^2 + 9A^2)}{16} = 1$$

$$\therefore A = \frac{1}{\sqrt{10}} \ . \tag{2.37}$$

The maximum PAPR for 16-QAM of four symbols at the corner constellation points out of the total 16 symbols can be evaluated as

$$PAPR_{16-QAM} = \frac{(9A^2 + 9A^2)}{1} = 1.8 = 2.55dB \ . \tag{2.38}$$

Similarly, the PAPR of the four inner constellations will be calculated as

$$PAPR_{16-QAM} = \frac{(A^2 + A^2)}{1} = 0.2 = -7dB \ . \tag{2.39}$$

For the remaining 8 constellation points, PAPR will be evaluated as

$$PAPR_{16-QAM} = \frac{(A^2 + 9A^2)}{1} = 1 = 0dB \ . \tag{2.40}$$

Once again, assuming a unit average power, the real and imaginary parts of 64-QAM take amplitude values of *A,3A,5A,7A,-A,-3A,-5A* and *-7A*, where *A* is give as

$$\frac{4(2A^2 + 2\times 10A^2 + 18A^2 + 2 + 26A^2 + 2\times 34A^2 \ldots + 3\times 50A^2 + 2 + 58A^2 + 2\times 74A^2 + 98A^2)}{64} = 1$$

$$\Rightarrow A = \frac{1}{\sqrt{42}} \ . \tag{2.41}$$

Then the maximum PAPR for 64-QAM of four corner symbols in the constellation out of a total of 64 symbols is calculated as

$$PAPR_{64-QAM} = \frac{(49A^2 + 49A^2)}{1} = 2.33 = 3.68dB \ . \tag{2.42}$$

It can be observed from the three equations that for a single OFDMA subcarrier transmission, QPSK, 16-QAM and 64-QAM will result in maximum PAPR of 0, 2.55, and 3.68 dB respectively. Simulation results of section 2.2.2 have also proved that the modulation order does not make much difference on the CCDF of PAPR when the number of parallel subchannels is large.

So far, we have focused on the importance of transmit power gains in increasing the uplink data rates. In wireless cellular system, transmission range and coverage extension improvements also deserve constant attentions as making the mobile networks access ubiquitous in some geographical areas has been a difficult task to achieve. The incremental range by a power gain of g_p dBs for a pathloss exponent *n* which is assumed to be between 2 and 4 depending on the wireless channel environment can be given as

$$\Delta R = \frac{r_2 - r_1}{r_1} = (10^{g_p/10})^{\frac{1}{n}} - 1 \ , \tag{2.43}$$

where r_1 is the original range and r_2 is the range with power gain of g_p dBs. Assuming a spherical-shape omni-cell, the gain in coverage area is given as

$$\Delta A = \frac{A_2 - A_1}{A_1} = \frac{4\pi r_2 - 4\pi r_1}{4\pi r_1} = (10^{g_p/10})^{\frac{2}{n}} - 1 \ . \tag{2.44}$$

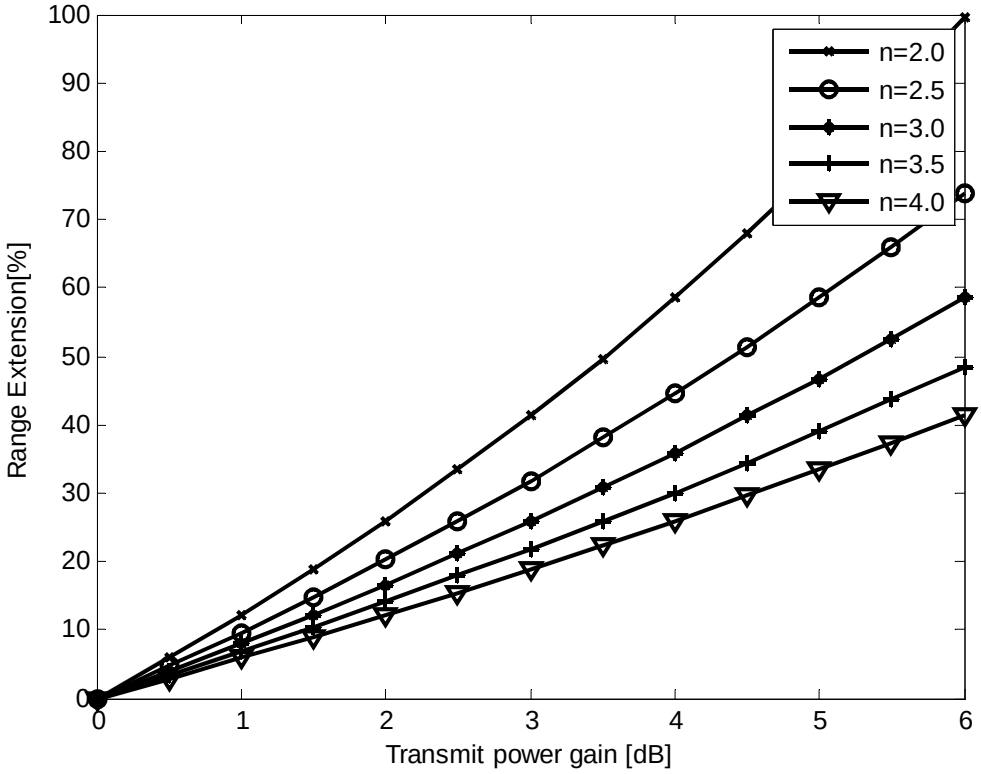

Figure 2.13. Range extension as a function of transmit power gain.

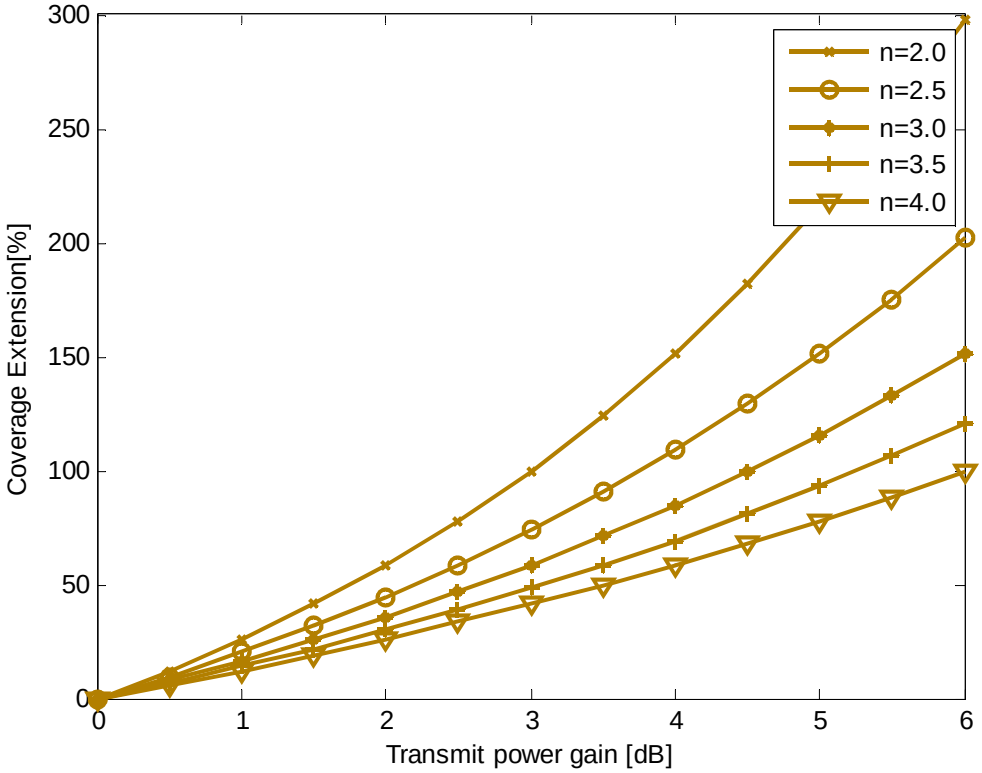

Figure 2.14. Coverage area gains as a function of transmit power gain.

From the above simulation results, it can be noted the incremental gains in the coverage area are as much 3 times larger than the range extension. Moreover, both incremental range extension and coverage area gains are larger at a smaller pathloss exponent for the same transmit power.

2.4. PAPR Reduction Techniques

Comparing with single-carrier systems, one of the detrimental effects of OFDMA transmission is the high PAPR which decreases the signal-to-quantization noise ratio of ADC and DAC and degrades the efficiency of the transmitter power amplifier (Khan

2009:86). This problem is very critical in uplink multiple access due to the limited battery of a mobile user.

2.4.1. Clipping and Filtering

The high PAPR problem in an OFDMA signal transmission can be mitigated by clipping the amplitude of the signal to a fixed level. This approach will help improve the signal-to-quantization noise ratio in ADC. In this technique, selecting an optimal clipping level and the number of quantization bits should be taken into account so that clipping distortion and quantization noise can be controlled, because low clipping level will result in a clipping distortion of the signal but decrease the PAPR and quantization noise , and vice versa (Cho, Kim, Yang & Kang 2010:222).

Referring back to figure 2.5, if an oversampling interpolation with oversampling factor L is implemented, the IFFT output signal $x[n]$ can be given as

$$x'[m] = \frac{1}{\sqrt{LN}} \sum_{k=0}^{LN-1} X'[k] e^{j2\pi m \Delta f k / LN}, m = 0,1,..., LN-1, \tag{2.45}$$

where $X'[k] = \begin{cases} X[k], \ 0 \le k < \frac{N}{2}, and\ LN - \frac{N}{2} < k < LN \\ 0, \ otherwise \end{cases}$, and Δf is a subcarrier spacing. For this scheme, the PAPR is redefined as

$$PAPR = \frac{\max\left|x'[m]^2\right|}{E(\left|x'[m]\right|^2)} \ . \tag{2.46}$$

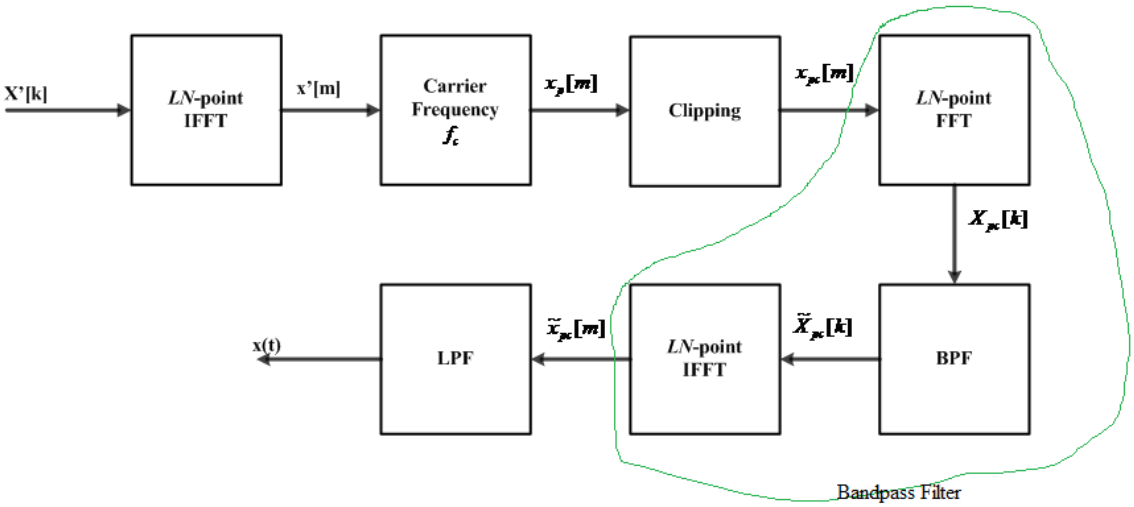

Figure 2.15. Block diagram of clipping and filtering in a PAPR reduction technique at the transmitter.

This block diagram shows that the oversampled discrete baseband OFDM signal $x'[m]$ is generated from the IFFT operation of $X'[k]$ with *N(L-1)* zero-padding in frequency domain and is then modulated with a carrier frequency f_c to produce a corresponding passband signal $x_p[m]$.It has been mentioned here that clipping is applied to reduce the effect of subcarriers' peak amplitudes. Thus, the clipped version of the passband signal is given as

$$x_{pc}[m] = \begin{cases} -A, & x_p[m] \le A \\ x_p[m], & |x_p[m]| < A \\ A, & x_p[m] \ge A \end{cases} = \begin{cases} x_p[m], if\ |x_p[m]| < A \\ \frac{x_p[m]}{|x_p[m]|}.A, & otherwise \end{cases}, \quad (2.47)$$

where A is a pre-fixed clipping level.

Note that clipping ratio is defined as the clipping level normalized by the rms value σ of an OFDM signal, such that $CR = \frac{A}{\sigma}$.

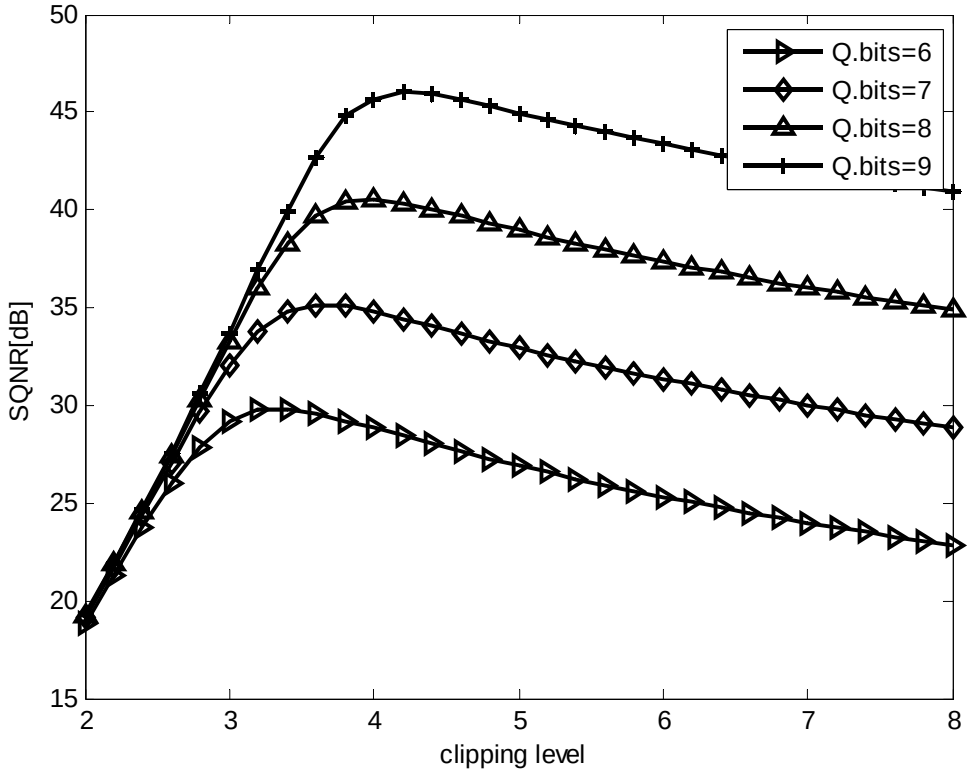

Figure 2.16. The effect of clipping on a quantized OFDM signal using 64-QAM with FFT size N=1024 and oversampling factor L=8.

The figure shows the values of SQNR of OFDMA signals with quantization bits of 6, 7, 8 and 9 against the clipping level. It can be observed that the optimal clipping level to maximize the SQNR varies with the quantization level.

Meanwhile it should be noted that clipping can cause out-of-band radiation which will result in signal interferences in adjacent channels by destroying orthogonality among the

subcarriers. Thus, to reduce this problem, the clipped signal needs to be filtered at the expense of peak amplitude regrowth.

3. MIMO SPATIAL CHANNEL MODELS IN LTE-ADVANCED

Because of the rapid rising demand of higher speed data transmission in the 21st Century telecommunications, multiple antenna systems have been intensively investigated and successfully deployed for the emerging broadband wireless access networks (Cho et al. 2010:263). To achieve this demand with high reliability, telecomm engineers have been busy finding techniques that help us actualize it.

The MIMO technology which was previously deemed interference paths is now used in wireless radio technologies to provide increased link capacity and spectral efficiency .This will reduce the error rate of a transmitted digital data by stabilizing the link and improving the signal performance. Since the maximum amount of data carried by a radio channel is limited by the Shannon's Law, MIMO spatial multiplexing is able to increase the user throughput by utilizing the multiple paths as additional channels to carry multiple versions of the same data.

3.1. Understanding MIMO

Modern radiocommunication networks are designed to continually provide higher data rates, and this is achieved by using multiple antenna technologies both at the transmitter and receiver as the classic communications like using higher modulation types or providing larger bandwidths is limited.

Classic communications use one transmit and one receive antenna, which is called SISO in MIMO technology. The capacity of this radio channel depends on the bandwidth B and the signal-to-noise ratio SNR , and according to the Shannon Law this capacity is given as:

$$C_{siso} = B \log_2 (1 + SNR) . \tag{3.1}$$

Figure 3.1. SISO antenna configurations.

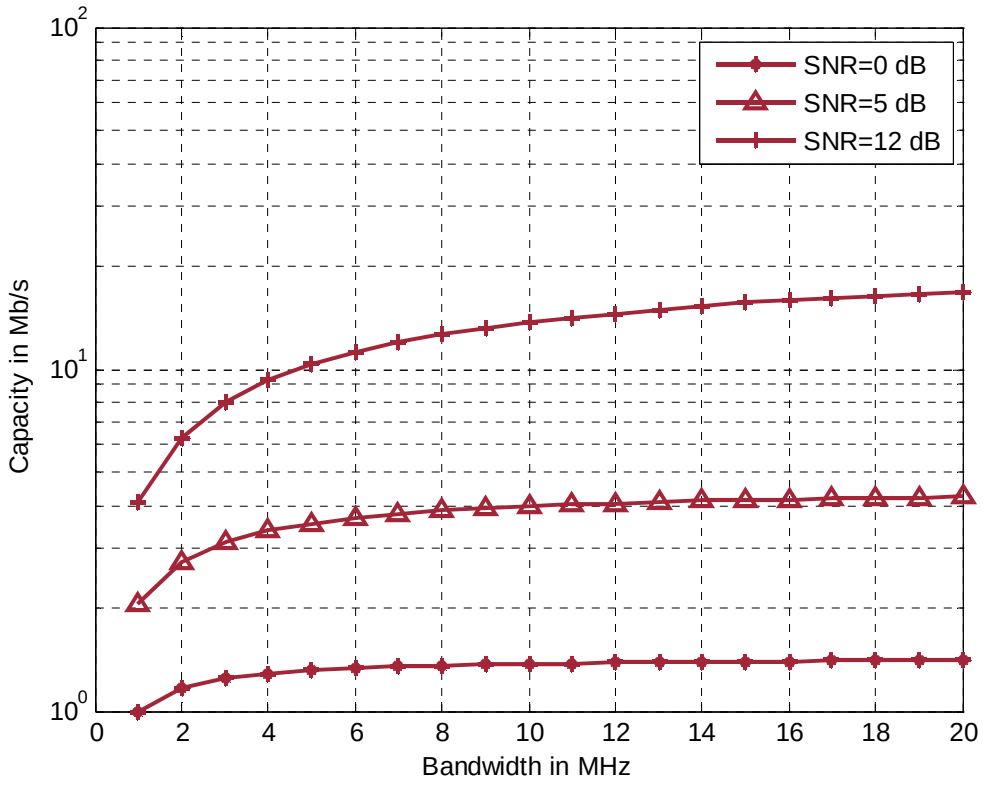

Figure 3.2. Shannon channel capacity with fixed power.

The above figure shows the effect of transmission bandwidths on a Shannon limited channel capacity when a transmit power is fixed. It can be observed that increasing bandwidth does not result in a linear increase in capacity if the transmission power is kept constant .Especially for the low SNR=0 dB, there is a small increase in capacity.

MIMO technology generally consists of multiple antennas at the transmitters and at the receivers as well. Assuming time-invariant and narrowband wireless MIMO channel, every antenna receives not only the direct components intended for it, but also the indirect components intended for the other antennas in the system.

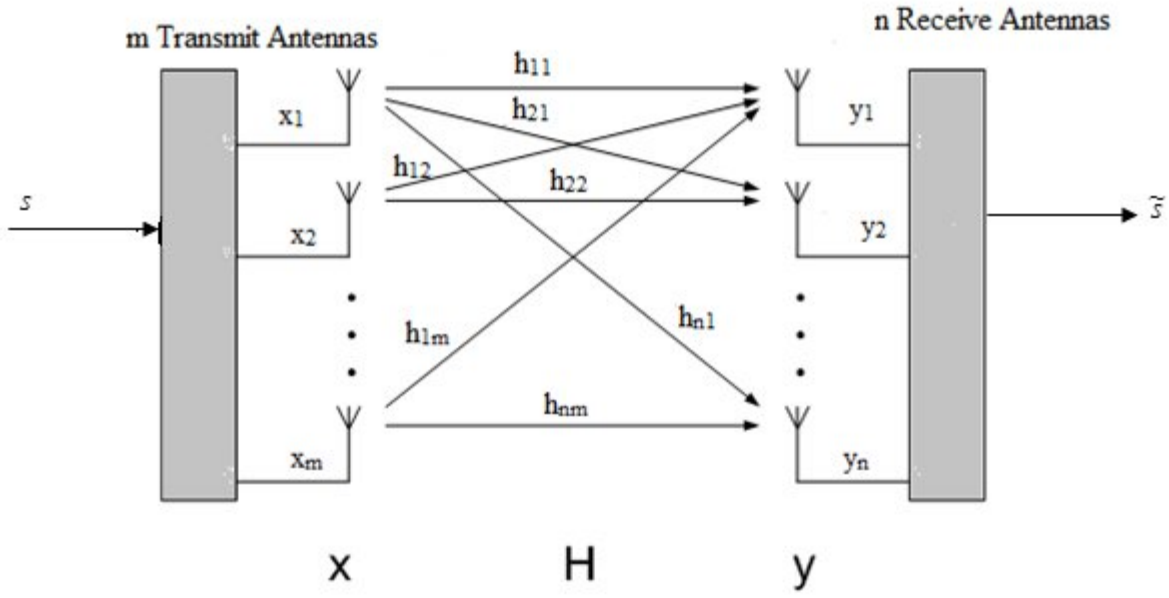

Figure 3.3. MIMO antenna configurations.

This MIMO technology helps us transmit the same symbol over all transmit antennas using different coding methods , and consequently it will alleviate deep fading which impairs the recovery of the transmitted symbol. From the above MIMO antenna configuration, the received signal at each receiving antenna can be represented as follows:

$$
\begin{aligned}
y_1 &= h_{11}x_1 + h_{12}x_2 + \ldots + h_{1m}x_m + z_1 \\
y_2 &= h_{21}x_1 + h_{22}x_2 + \ldots + h_{2m}x_m + z_2 \\
&\vdots \\
y_n &= h_{n1}x_1 + h_{n2}x_2 + \ldots + h_{nm}x_m + z_n
\end{aligned}
\tag{3.2}
$$

3.1.1. Parallel decomposition of spatial multiplexing MIMO channels

In asymmetrical antenna constellations ($m \neq n$), the number of independent data streams K to be transmitted over uncorrelated parallel channels is always less than or equal to the minimum number of antennas at the transmitter and the receiver. For instance, in a 4x4 MIMO structure a maximum of 4 independent data streams can be transmitted, while in a 2x3 MIMO structure, a maximum of 2 independent data streams can be transmitted. Theoretically, the capacity of this technology increases linearly K more times than that of a single antenna system (Koivo & Elmusrati 2009: 298-301). Then it is represented as

$$C_{mimo} = K * B\log_2(1 + SNR) \ . \tag{3.3}$$

It is possible to mathematically prove the number of parallel independent spatial multiplexing MIMO channels. This is obtained by a linear transformation of the input vector $\tilde{x}$ to the channel input to the antennas x and the output vector $\tilde{y}$ to the channel output y through *transmitter precoding* and *receiver shaping* respectively (see figure 3.4). Consider a MIMO channel with the channel matrix *H* known to both the transmitter and the receiver. In linear algebra, the singular value decomposition $[U, \Lambda, V] = svd(H)$ produces a

diagonal matrix Λ of non-negative singular values σ_i and with the same dimension as H, and two unitary matrices U and V, with dimensions $n \times n$ and $m \times m$ respectively so that

$$H = U\Lambda V^H. \tag{3.4}$$

Note that $\sigma_i = \sqrt{\lambda_i}$, where λ_i is the i^{th} eigenvalue of HH^H. The rank of H corresponds to the non-zero singular values, that is, $rank(H) \le K$. The singular values are the diagonal elements of Λ in decreasing order.

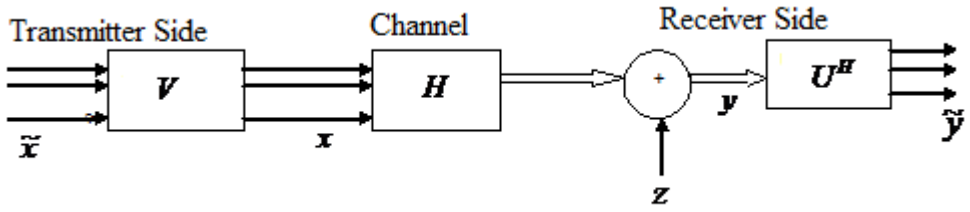

Figure 3.4. Transmitter precoding and receiver shaping.

It can be seen from the above figure that in transmitter precoding $x = V\tilde{x}$, and in receiver shaping $\tilde{y} = U^H y$. Then the output signal in the receiver can be expressed as

$$\begin{aligned}
\tilde{y} &= U^H(Hx + z) \\
&= U^H(U\Lambda V^H x + z) \\
&= U^H(U\Lambda V^H V\tilde{x} + z) \\
&= U^H U\Lambda V^H V\tilde{x} + U^H z \\
&= I_n \Lambda I_m \tilde{x} + U^H z \\
&= \Lambda\tilde{x} + \tilde{z}
\end{aligned} \tag{3.5}$$

Equation (3.5) clearly shows that the MIMO channel is decomposed into K independent SISO channels where the channel has input $\tilde{x}_i$, output $\tilde{y}_i$, noise $\tilde{z}_i$, and channel gain σ_i for $i = 1,2,3,...,K$.

3.1.2. Spatial Diversity

MIMO systems can be used to increase data rates through multiplexing and improve performance (robustness) through diversity. There are several diversity techniques in use today to make radiocommunications more robust even with time-varying channels. These include:

- Time diversity with different time slots and channel coding ;
- Frequency diversity with different channels, spread spectrum and OFDM;
- Spatial diversity which requires the use of MIMO antennas at the transmitter or the receiver end (Cho et al. 2010:281-283).

Diversity technique is aimed at making the transmission more reliable by transmitting redundant data on different paths intending to receive the same information-bearing signals. This technique is done by converting Rayleigh fading channel into more stable AWGN-like channel without any devastating signal fading. The receiver diversity uses multiple antennas on the receiver side, while the transmitter diversity uses multiple antennas at transmitter side.

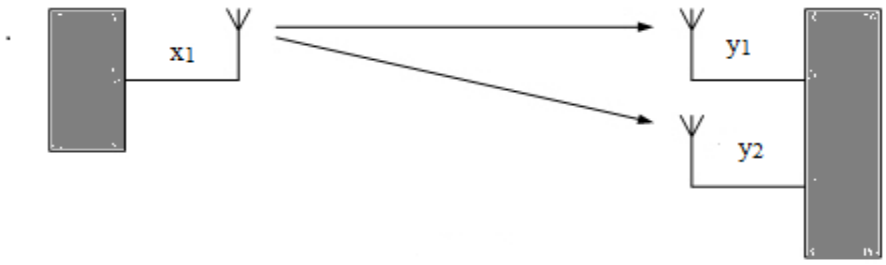

Figure 3.5. SIMO antenna configurations.

In this case, the receiver sees two differently faded signals coming from the two different paths. Then the SNR can be increased by using appropriate diversity decoding techniques in the receiver, for example, switched diversity which selects a stronger signal and MRC which uses the optimal weights to combine the signals (Sklar 2001: 983-986).

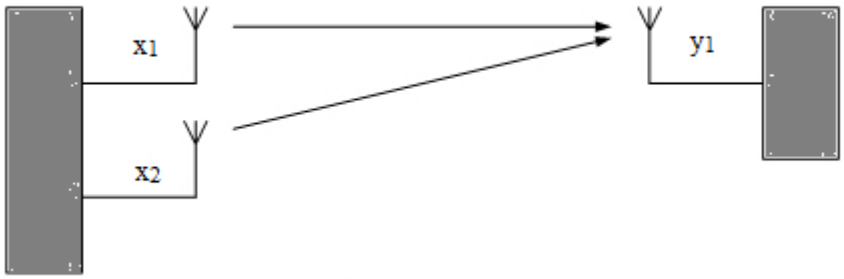

Figure 3.6. MISO antenna configurations.

In MISO antenna configurations, the same data is transmitted redundantly over the transmit antennas so that these multiple antennas and redundancy coding are moved from the mobile station to the base station where it is simpler and cheaper to implement. This will enable cellphone UEs to save battery consumption.

3.2. MIMO Channel Capacity

Given the received symbol vector $y \in C^{n\times 1}$, transmitted symbol vector $x \in C^{m\times 1}$, the transmission channel gain matrix H and noise vector $z \in C^{n\times 1}$, the matrix form representation of the equation (3.2) is

$$y=Hx+z, \tag{3.6}$$

where H is the $n \times m$ matrix with the channel gains h_{ij} representing the gain from transmit antenna j to receive antenna i. Given SVD of H, the following Eigen-decomposition holds:

$$HH^H = U\Lambda\Lambda^H U^H = Q\Sigma Q^H . \tag{3.7}$$

, where $Q = U$ Such that $QQ^H = I_n$,and Σ is a diagonal matrix of dimension $n \times n$.

Channel capacity is determined by the channel gain matrix information or its distribution at the transmitter and /or the receiver. Consider a time-varying channel with random matrix H known to the receiver. The capacity of such a random MIMO channel structure is given by the formula:

$$C_{MIMO} = BE_H[\log_2 \det(I_n + \frac{1}{N_0 B} HR_x H^H)], \tag{3.8}$$

where $R_x = E[xx^H]$ is the autocorrelation of the transmitted signal vector and N_0 is the power spectral density of the additive noise. If there is no channel information at the transmitter, the maximum transmit power $P_{\max}$ is equally divided among all transmit antennas and independent symbols are sent over the different channels. Hence, the optimum input covariance that maximizes the capacity is given as

$$R_x = \frac{P_{\max}}{m} I_m = diag(p_1, p_2, ..., p_m). \tag{3.9}$$

When the power at each transmit antenna is assumed to be unity, then it is obvious that $trace(R_x) = sum(diag(R_x)) = m$, that is, $P_{\max} = \sum_{i=1}^{m} p_i = m$, which is a power constraint.

For any matrices $A^{k_1 \times k_2}$ and $B^{k_1 \times k_2}$, the following identity holds:

$$\det(I_{k_1} + AB) = \det(I_{k_2} + BA).$$

Then, equation (3.8) is written as

$$\begin{aligned}
C_{MIMO} &= BE_H[\log_2 \det(I_n + \frac{P_{\max}}{mN_0 B} HH^H)] \\
&= BE_H[\log_2 \det(I_m + \frac{p_{\max}}{mN_0 B} H^H H)] \\
&= BE_H[\log_2 \det(I_m + \frac{p_{\max}}{mN_0 B} Q\Sigma Q^H)] \\
&= BE_H[\log_2 \det(I_m + \frac{P_{\max}}{mN_0 B} Q^H Q\Sigma)] \\
&= BE_\Sigma[\log_2 (I_m + \frac{p_{\max}}{mN_0 B} \Sigma] \\
&= BE_\lambda[\log_2 \prod_{i=1}^{m} (1 + \frac{P_{\max}\lambda_i}{mN_0 B})] \\
&= B\sum_{i=1}^{m} E_{\lambda_i} [\log_2 (1 + \frac{P_{\max}\lambda_i}{mN_0 B})] \\
&= B \sum_{i=1}^{\min(m,n)} E_{\lambda_i} [\log(1 + \frac{P_{\max}\lambda_i}{mN_0 B})].
\end{aligned} \tag{3.10}$$

To enhance the reliability of the system, we have to optimize the power allocated at each transmit antenna. The capacity C_{MIMO} can be further maximized by solving the following equation using Lagrangian optimization technique:

$$C_{MIMO} = B \times E_{\lambda}[\sum_{i=1}^{m} \log_2(1 + \frac{p_i \lambda_i}{mN_0 B})]$$

$$\text{subject to } \sum_{i=1}^{m} p_i \leq P_{\max} \ . \tag{3.11}$$

Then the solution to this optimization is *water-filling power allocation algorithm*, which states that more power must be allocated to the mode with higher SNR. If an SNR is below the threshold, no power is allocated to the corresponding modes because they must not be used.

$$p_i^{\ opt} = (\mu - \frac{mN_0 B}{\lambda_i})^+$$

$$\text{and } \sum p_i^{\ opt} = P_{\max} \quad , \tag{3.12}$$

where μ is the SNR threshold.

Whereas the capacity of deterministic MIMO channel is given as

$$C_d = B\sum_{i=1}^{m} \log_2(1 + \frac{P_{\max} \lambda_i}{mN_0 B}) \ . \tag{3.13}$$

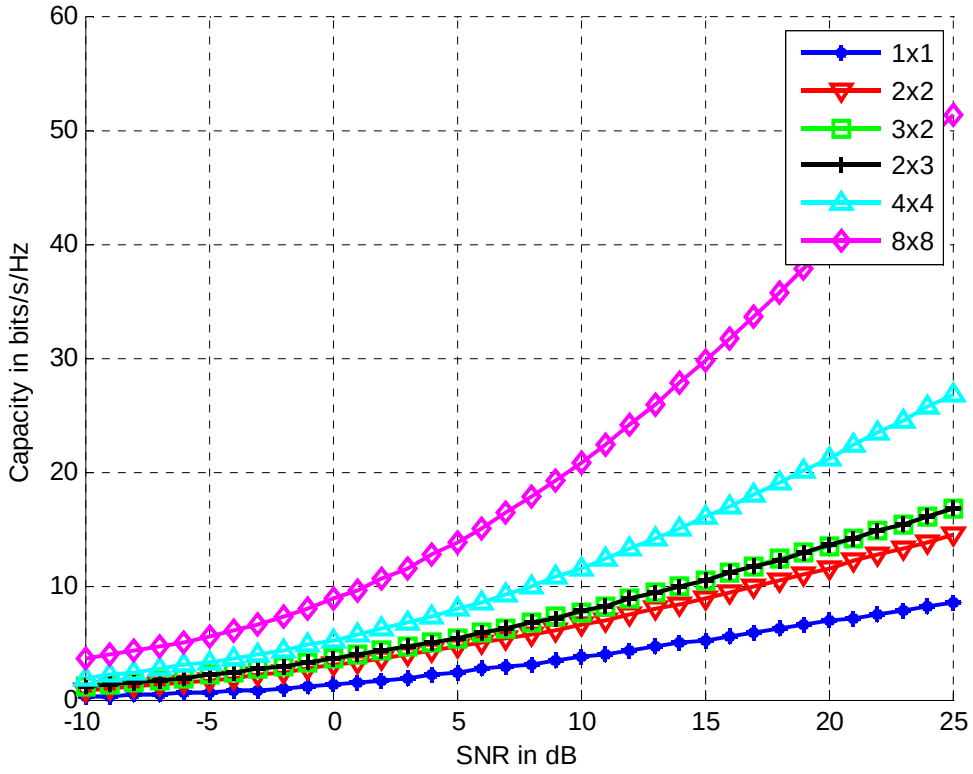

Figure 3.7. Deterministic MIMO channel capacity with different antenna configurations when channel information known to both sides (Bandwidth B=1.4 MHz).

The simulation result shows that spatial multiplexing increases the data rate as the data is divided into separate streams which are transmitted independently via separate antennas. It can also be observed that the LTE-Advanced data rate demand of up to 1Gbits/s in the downlink transmission is achieved with 8×8 MIMO antenna configurations. For instance, if the given bandwidth is 20 MHz, then the date rate is calculated to be 1 Gbits/s for the peak spectrum efficiency of about 50 bits/s/Hz with 8×8 MIMO configurations. It is also worth seeing in the plot that antenna configurations of 3×2 and 2×3 have the same capacity, which proves that in an asymmetrical antenna constellation, the number of independent data streams to be transmitted in a MIMO channel is equal to the minimum the number of antenna configuration.

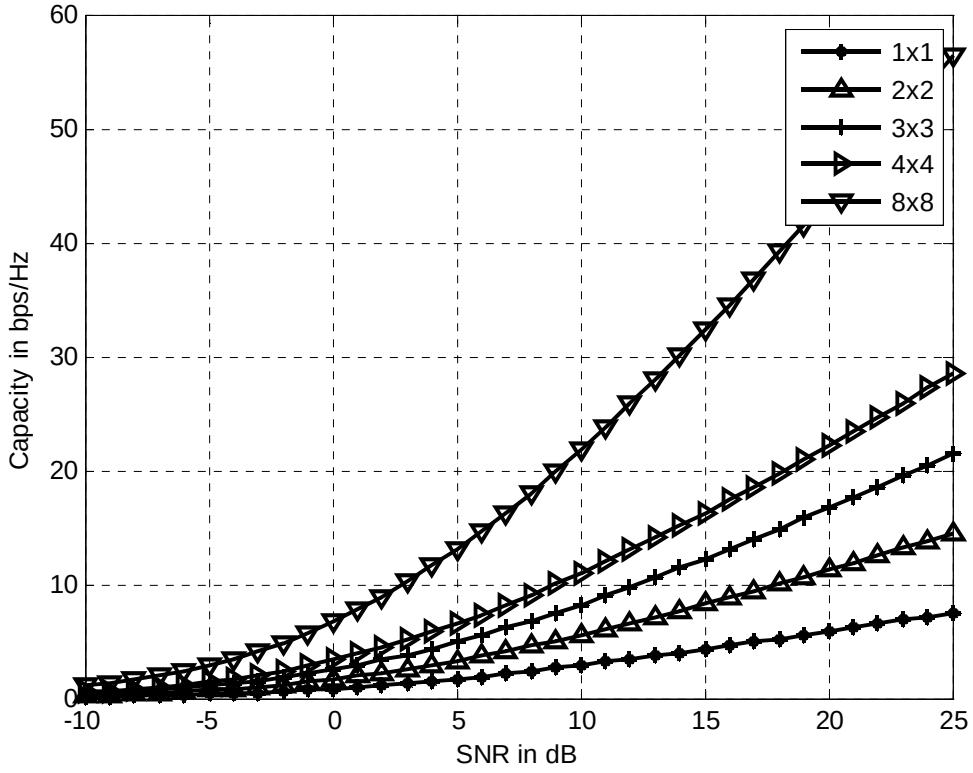

Figure 3.8. Random MIMO channel capacity when channel information is not available at the transmitter.

The simulation result clearly shows the MIMO channel capacity improves with increasing the number of antenna configurations at the transmitter and the receiver irrespective of the unavailability of channel information at the transmitter. This scenario makes difference only when one wants to allocate a reasonable power to every transmitter depending on the channel conditions that may have impacts on the performance of the system.

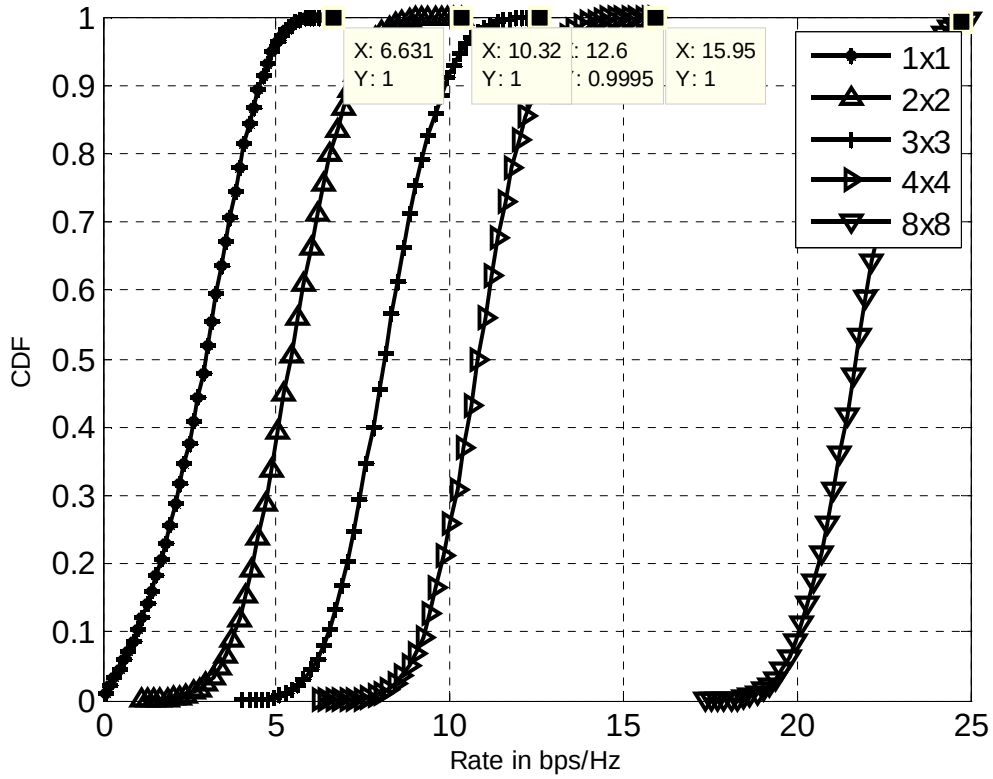

Figure 3.9. Distribution of MIMO channel capacity when channel information is not available at the transmitter and $SNR = 10\,\text{dB}$.

The plot of the distribution of the random MIMO channel capacity shows that the values of the spectral efficiency at CDF of 1% with antenna structures of 1×1, 2×2, 3×3, 4×4 and 8×8 are 6.631, 10.32, 12.6, 15.95 and 25 bps/Hz, respectively. This confirms that a MIMO channel with the highest antenna configuration has a larger capacity than those with fewer configurations.

3.3. SU-MIMO

This system exploits multiple antennas at the transmitter and the receiver to improve the data rate, robustness and resistance to interferences. In LTE-Advanced, the SU-MIMO antenna configurations for the downlink and the uplink are up to 8 and 4 transmit antennas, respectively.

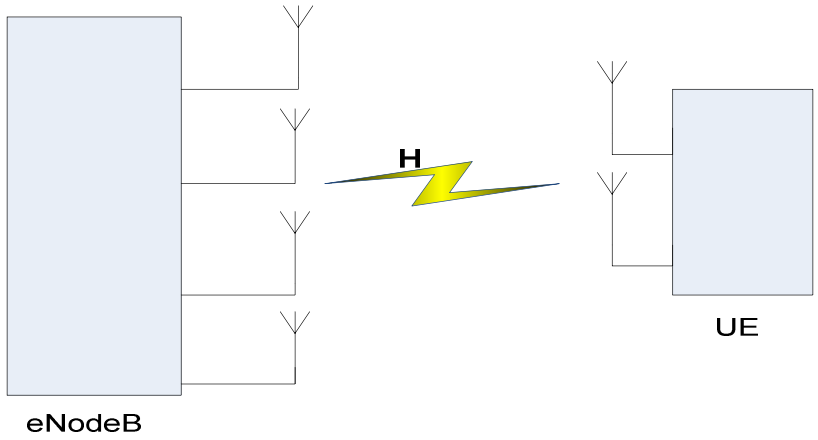

Figure 3.10. SU-MIMO antenna configuration.

3.4. MU-MIMO

In this system, the base station communicates with multiple users, in which it sends different information streams to several users on the downlink broadcast channel, and receives different information from the users on the uplink multiple access channel.

On the downlink, MU-MIMO is of great importance in 3GPP LTE-Advanced because the capacities of MIMO channels can be maximized with a multiple antenna base station also known as eNodeB and a number of single antenna mobile users. Moreover, the complexity of on the UE side can be minimized by using only one transmit antenna.

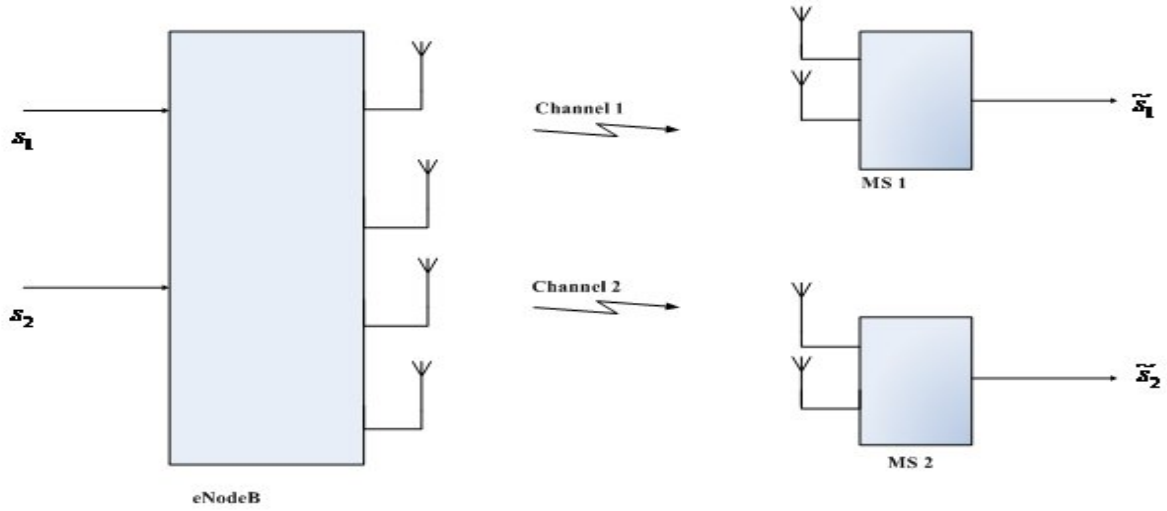

Figure 3.11. Downlink of a MU-MIMO network.

4. MIMO CHANNEL ESTIMATIONS IN LTE-ADVANCED

The recent dramatic increase of mobile data usage and the emergence of new applications such as online gaming and mobile stream contents have motivated the 3GPP to work toward developing LTE-Advanced which is expected to substantially improve user throughput ,sector capacity ,spectrum efficiency and reduce latency. In order to satisfy the requirements of these various applications, significant technological achievements are required to ensure that wireless devices have appropriate architectures suitable for supporting a wide range of services delivered to the users. One of these achievements is the introduction of MIMO wireless architectures which are capable of providing significant improvements over the classical communications.

According to Hanzo, Akhtman, Wang & Jiang (2011:2), MIMO capacity theoretically increases linearly with the number of transmit antennas provided that the number of receive antennas is equal to the number of transmit antennas .This linear capacity increase is obviously achieved up on increasing transmit power as the total transmit power is increased proportionately to the number of transmit antennas. In fact this is very beneficial, since the Shannon Law states that channel capacity increases only logarithmically with the transmit power. However, under realistic conditions, the linearity cannot be realized due to multichannel fading which causes the symbols to interfere, which in turn causes poor performance in a communication system. The fading effects can be mitigated by using MIMO channels equalizations. Thus, in this paper, MMSE, ZF and ZF-SIC equalizers will be investigated. Of course, the performance of these three equalizers will be compared in a Rayleigh fading channel to finally recommend the best technique for 4G LTE-Advanced.

In 4G mobile technologies, the MIMO schemes E-UTRA for the sets of antenna configurations would be: 2, 4, or 8 transmit antennas and a minimum of 2 receive antennas in the downlink, and 1, 2, or 4 transmit antennas with a minimum of 2 receive antennas in the uplink (Li, Li, Lee, Lee ,Mazzarese ,Clerckx & Li 2009).

4.1. Channel Model

Let the pulse symbols to transmit be represented as

$$x(t) = \sum_{m=-\infty}^{\infty} a_m g(t - nT) \ , \tag{4.1}$$

where T is the symbol period, a_m is the symbol to transmit, $g(t)$ is the transmit pulse shaping filter, and m is the symbol index. Here, for the sake of simplicity, the transmit pulse shaping filter is assumed to be the delta function, that is, $g(t) = \delta(t)$ so that the discrete time signal $x[k] = a_m$.

Consider a Rayleigh multipath fading channel with sampling space $T_s : h[kT_s] = [h_1 \ h_2 \ \ h_3 ...]$, where k is the index of the sampling time, and h_1, h_2, and h_3 are the channel impulses at times 0, T_s and $2T_s$ respectively. The received signal in frequency domain is given as

$$y[k] = x[k] \otimes h[k] + z \ , \tag{4.2}$$

where $x[k]$ is discrete transmit symbol, and z is AWGN with mean $\mu = 0$ and, variance $\sigma^2 = \frac{N_0}{2}$.

In multipath environment, an impulse transmitted from the transmitter will reach the receiver as a train of impulses. If the transmit bandpass signal is given as

$$x(t) = \Re\{x_b(t) e^{j 2\pi f_c t}\} \ , \tag{4.3}$$

where $x_b(t)$ is the baseband signal , and f_c is the carrier frequency, then the received signal through multiple paths is represented as

$$y(t) = \sum_n \alpha_n(t) x(t - \tau_n(t)), \tag{4.4}$$

where $\alpha_n(t)$ is the attenuation, $\tau_n(t)$ is the delay and n is the number of the paths. Substituting equation (4.3) into equation (4.4), the received signal will be expressed as

$$y(t) = \Re\{\sum_n \alpha_n(t) x_b(t - \tau_n(t)) e^{j2\pi f_c(t-\tau_n(t))}\}. \tag{4.5}$$

The baseband equivalent of the received signal is given as

$$\begin{aligned} y_b(t) &= \sum_n \alpha_n(t) x_b(t - \tau_n(t)) e^{-j2\pi f_c \tau_n(t)} \\ &= \sum_n \alpha_n(t) x_b(t - \tau_n(t)) e^{-j\beta_n(t)}, \end{aligned} \tag{4.6}$$

where $\beta_n(t) = 2\pi f_c \tau_n(t)$ is the phase of the n^{th} path. The phase of each path can change by 2π radians when the delay $\tau_n(t)$ changes by $\frac{1}{f_c}$. If f_c is large, relative small motions in the medium can cause change of 2π radians. Since the distance between the transmitter and the receiver is much larger than the wavelength of the carrier frequency, the phase is uniformly distributed over [0 2π], and the phases of each path are independent (Tse & Viswanath 2005:59-60).

When there are a large number of paths with circularly symmetric complex Gaussian random variable, by applying Central Limit Theorem it is modeled as Rayleigh fading channel. This symmetric Gaussian variable can be represented as $Z=X+jY$, where the real and imaginary parts are zero mean independent and identically distributed Gaussian random variables, such that $E[Z] = E[e^{j\varphi} Z] = e^{j\varphi} E[Z]$ and $\sigma^2 = E[Z^2]$. Then the

magnitude |Z| which has a probability density function, $p(z) = \frac{z}{\sigma^2} e^{\frac{-z^2}{2\sigma^2}}, z \geq 0$, is called a *Rayleigh random variable*.

4.2. MIMO with MMSE Equalizer

MMSE equalizer minimizes the mean square error, which is a commonly used measure of estimator quality. Then in this channel estimation technique, a set of equalization coefficients $c[k]$ needs to be determined for each sample index *k* to minimize the error between the desired and the equalized signals.

$$\begin{aligned} E(e[k])^2 &= E(x[k] - c[k] \otimes y[k])^2 \\ &= E((x[k] - c^T y)(x[k] - c^T y)^T) \\ &= E(x[k]^2 - E(c^T yx[k]) - E(x[k]y^T c) + E(c^T yy^T c) \\ &= E(x[k]^2) - c^T R_{yx} - R_{xy} c + c^T R_{yy} c \ , \end{aligned} \tag{4.7}$$

where $e[k]$ is a set of sample errors, $c[k]$ is a set of equalization coefficients of dimension [K×1], $y[k]$ is a set received samples of dimension [K×1], K is the number of taps of the equalizer, R_{yx} & R_{xy} are the cross-correlations between the received and transmitted samples, and R_{yy} is the auto-correlation of the received sample.

To find the equalization coefficients, the following first order differential equation needs to be solved by setting to zero because the value equation (4.7) at c is less than any value in its immediate neighborhood.

$$\frac{\partial}{\partial c}\{E(e[k]^2)\} = 0$$

$$\Rightarrow \frac{\partial}{\partial c}\{E(x[k]^2) - c^T R_{yx} - R_{xy}c + c^T R_{yy}c\} = 0 \tag{4.8}$$

$$\Rightarrow -R_{xy} + R_{yy}c = 0$$

$$\Rightarrow c = R_{yy}^{-1} R_{xy}$$

Simplifying R_{xy} and R_{yy}, the following equations will be found:

$$\begin{aligned} R_{xy} &= E(x[k]y^T) \\ &= E(x[k](hx[k]+z)^T) \\ &= h^T E(x^2[k] + x[k]z) \\ &= h^T \{E(x^2[k] + E(x[k]z)\} \\ &= h^T \end{aligned} \tag{4.9}$$

$$\begin{aligned} R_{yy} &= E(yy^T) \\ &= E\{(hx[k]+z)(hx[k]+z)^T\} \\ &= E(hh^T)E(x^2[k]) + hE(x[k]z) + h^T E(x[k]z + E(z^2) \\ &= E(hh^T) + E(z^2) \end{aligned} \tag{4.10}$$

Note that $E(x^2[k]) = 1$, which is the input variance of the normalized average signal power, and $E(x[k]z) = 0$ because there is no correlation between the transmitted signal and the noise. Finally, the equalization coefficient is expressed as

$$c = \{E(hh^T) + E(z^2)\}^{-1} h^T . \tag{4.11}$$

In MMSE signal detection, the weight matrix helps us maximize SINR after the detection is given as

$$W_M = (H^H H + \sigma_z{}^2 I)^{-1} H^H \ . \tag{4.12}$$

The channel response has to be inverted by the weight matrix to detect the signals from each transmit antenna.

$$\begin{aligned} \tilde{x}_M &= W_M y \\ &= W_M (Hx + z) \\ &= \tilde{x} + (H^H H + \sigma_z{}^2 I)^{-1} H^H z \\ &= \tilde{x} + \tilde{z}_M \ . \end{aligned} \tag{4.13}$$

Using the SVD equation (3.4), the noise power after signal detection is evaluated as

$$\begin{aligned} \left\| \tilde{z}_M \right\|_2{}^2 &= \left\| (H^H H + \sigma_z{}^2 I)^{-1} H^H z \right\|^2 \\ &= \left\| (V \Lambda^2 V^H + \sigma_z{}^2 I)^{-1} V \Lambda U^H z \right\|^2 \end{aligned}$$

$$= \left\| (V\Lambda^2 V^H + {\sigma_z}^2 I)^{-1} (\Lambda^{-1} V^H)^{-1} U^H z \right\|^2$$

$$= \left\| (\Lambda\, V^H + {\sigma_z}^2 \Lambda^{-1} V^H)^{-1} U^H z \right\|^2$$

$$= \left\| V(\Lambda\ + {\sigma_z}^2 \Lambda^{-1})^{-1} U^H z \right\|^2 . \qquad (4.14)$$

Remember that $\|Vx\|^2 = \|x\|^2$, where V is a unitary matrix. Then the expected value of a random noise power is expressed as

$$E[\|\tilde{z}_M\|_2^{\ 2}\ ] = E[\left\| V(\Lambda\ + {\sigma_z}^2 \Lambda^{-1})^{-1} U^H z \right\|^2]$$

$$= E[tr((\Lambda + {\sigma_z}^2 \Lambda^{-1})^{-1} U^H z z^H U (\Lambda + {\sigma_z}^2 \Lambda^{-1})^{-1})]$$

$$= tr((\Lambda + {\sigma_z}^2 \Lambda^{-1})^{-1} U^H U E[zz^H] (\Lambda + {\sigma_z}^2 \Lambda^{-1})^{-1})$$

$$= tr((\Lambda + {\sigma_z}^2 \Lambda^{-1})^{-1} E[zz^H] (\Lambda + {\sigma_z}^2 \Lambda^{-1})^{-1})$$

$$= tr((\Lambda + {\sigma_z}^2 \Lambda^{-1})^{-1} {\sigma_z}^2 (\Lambda + {\sigma_z}^2 \Lambda^{-1})^{-1})$$

$$= tr({\sigma_z}^2 (\Lambda + {\sigma_z}^2 \Lambda^{-1})^{-2})$$

$$= \sum_{i=1}^{m} {\sigma_z}^2 (\sigma_i + \frac{{\sigma_z}^2}{\sigma_i})^{-2}$$

$$= \sum_{i=1}^{m} \frac{{\sigma_z}^2 {\sigma_i}^2}{({\sigma_i}^2 + {\sigma_z}^2)^2} \ = \sum_{i=1}^{m} \frac{\lambda_z \lambda_i}{(\lambda_i + \lambda_z)^2} \ . \qquad (4.15)$$

4.3. MIMO with ZF Equalizer

ZF equalizer applies the inverse of the frequency response of the channel to the received signal so that the signal after the channel can be recovered. In signal detection process, except the desired signal from the target transmit antenna, all other signals are obviously treated as interferences (Cho et al. 2010: 319-323). These interference signals will be either minimized by MMSE equalizer or nullified by ZF equalizer. Thus, the ZF equalizer nullifies the interference by the weight matrix which is given as

$$W_{ZF} = (H^H H\ )^{-1} H^H . \tag{4.16}$$

To facilitate the detection of the desired signals from each transmit antenna, the channel response is inverted by the weight matrix.

$$\begin{aligned} \tilde{x}_{ZF} &= W_{ZF} y \\ &= x + (H^H H)^{-1} H^H z \\ &= \tilde{x} + \tilde{z}_F \end{aligned} \tag{4.17}$$

It is clear that the error performance is directly related to the noise power $\left\|\tilde{z}_F\right\|_2^{\ 2}$. Using the SVD equation (4.4), the noise power after signal detection is evaluated as

$$\left\|\tilde{z}_F\right\|_2^{\ 2} = \left\|(H^H H)^{-1} H^H z\right\|^2$$

$$= \left\| (V\Lambda^2 V^H)^{-1} V\Lambda U^H z \right\|^2$$

$$= \left\| V\Lambda^{-2} V^H V\Lambda U^H z \right\|^2$$

$$= \left\| V\Lambda^{-1} U^H z \right\|^2 . \qquad (4.18)$$

Again remember that $\|Vx\|^2 = x^H V^H Vx = x^H x = \|x\|^2$ for a unitary matrix V, the expected value of the noise power is given as

$$E[\|\tilde{z}_F\|_2^{\,2}] = E[\|\Lambda^{-1} U^H z\|_2^{\,2}]$$

$$= E[tr(\Lambda^{-1} U^H z z^H U \Lambda^{-1})]$$

$$= tr(\Lambda^{-1} U^H E[zz^H] U \Lambda^{-1})$$

$$= tr(\sigma_z^{\,2} \Lambda^{-1} U^H U \Lambda^{-1})$$

$$= \sigma_z^{\,2} tr(\Lambda^{-2})$$

$$= \sum_{i=1}^{m} \frac{\sigma_z^{\,2}}{\sigma_i^{\,2}} = \sum_{i=1}^{m} \frac{\lambda_z}{\lambda_i} \ . \qquad (4.19)$$

In the course of linear equalization filtering, the noise power is enhanced when the condition number of channel matrix is large, causing the minimum singular value to be very small. Then for $\sigma_{\min}^{\,2} = \min(\sigma_1^{\,2}, \sigma_2^{\,2}, ..., \sigma_m^{\,2})$, equations (4.15) and (4.19) are respectively given as

$$E[\|\tilde{z}_M\|_2^{\,2}] = \frac{\sigma_z^{\,2} \sigma_{\min}^{\,2}}{(\sigma_{\min}^{\,2} + \sigma_z^{\,2})^2} \quad , \qquad (4.20a)$$

and $$E[\|\tilde{z}_F\|_2^2] = \frac{\sigma_z^2}{\sigma_{\min}^2}. \quad (4.20b)$$

By comparing the above two equations, it can be clearly seen that the effect of noise enhancement in MMSE filtering is less critical than that of in ZF filtering. In fact, this can be proved by finding the relation between the two equations as follows:

$$\frac{E[\|\tilde{z}_F\|_2^2]}{E[\|\tilde{z}_M\|_2^2]} = \frac{\sigma_z^2/\sigma_{\min}^2}{\sigma_z^2\sigma_{\min}^2/(\sigma_z^2+\sigma_{\min}^2)^2}$$

$$= (1+\frac{\sigma_z^2}{\sigma_{\min}^2})^2.$$

4.4. Evaluation of Average Probability of Bit Error in QPSK Modulations

Since the performance of a digital communication system is usually evaluated in terms of the probability of bit error against the level of the SNR of the signal, it is very important to deal with the average probability of bit error in QPSK and QAM modulations. Let the value of bit energy to noise ratio be E_b / N_0. Then according to Haykin (2001:497); Proakis (2000:269); Sklar (2001:223-224), the probability of bit-error rate for a QPSK modulated symbol is given as

$$P_b = \frac{1}{2} erfc[\sqrt{(E_b / N_0)}] . \quad (4.21)$$

Due to the presence of the channel impulse *h*, the instantaneous bit energy to noise ratio becomes $\frac{|h|^2 E_b}{N_0}$. Hence, the probability of error for a given value of *h* is expressed as

$$P_{b/h} = \frac{1}{2} erfc\left(\sqrt{\frac{|h|^2 E_b}{N_0}}\right) = \frac{1}{2} erfc(\sqrt{\beta}), \tag{4.22}$$

where $\beta = \frac{|h|^2 E_b}{N_0}$.

It has been mentioned that the channel is assumed to be a Rayleigh fading channel; thus, $|h|$ is a Rayleigh distributed random variable, while $|h|^2$ is a Chi-square random variable with two degree of freedom. Then the conditional PDF of the Chi-square distribution for a random variable β is given as

$$P(\beta) = \frac{1}{(E_b / N_0)} e^{-\beta/(E_b/N_0)} = \frac{1}{\overline{\beta}} e^{-\frac{\beta}{\overline{\beta}}}, \tag{4.23}$$

where $\overline{\beta} = E_b / N_0$.

The resulting average probability of error for any random values of $|h|^2$ must be calculated by evaluating the conditional PDF $P_{b/h}$ over the PDF of β. It is given as

$$P_b = \int_0^{\infty} \frac{1}{2} erfc(\sqrt{\beta}) \times P(\beta) d\beta$$

$$= \frac{1}{2}\left(1 - \sqrt{\frac{E_b / N_0}{(E_b / N_0) + 1}}\right) . \qquad (4.24)$$

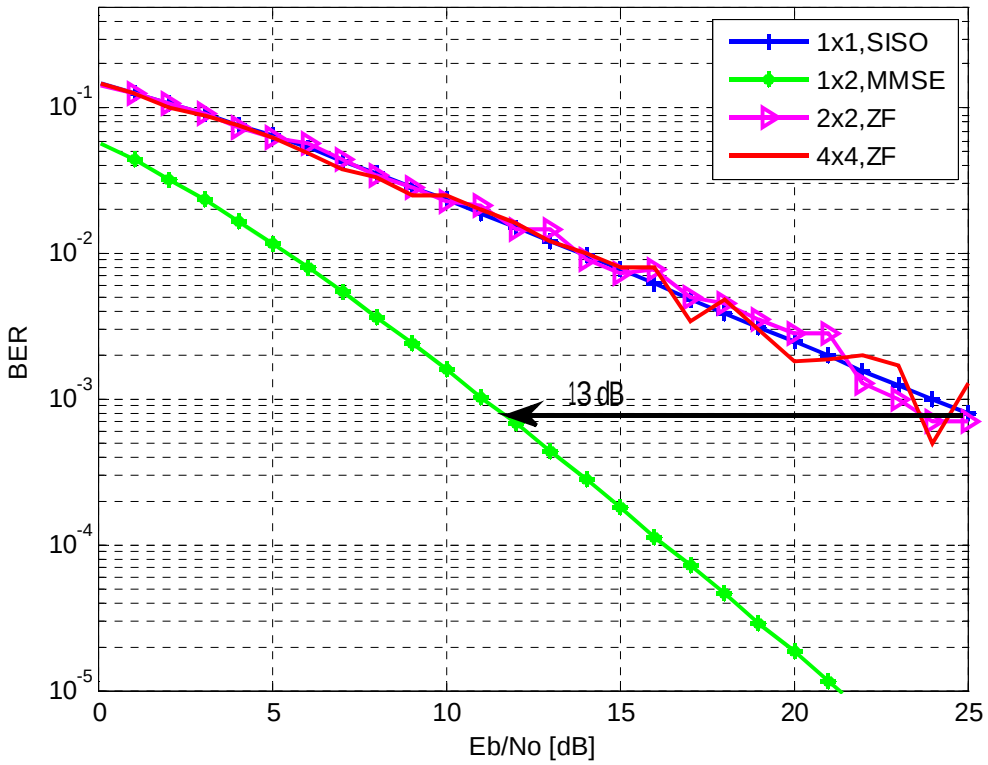

Figure 4.1. BER Comparison for MMSE and ZF using different MIMO configurations using QPSK (number of taps=7).

The plot shows the BER performance of MMSE and ZF equalizers with different MIMO configurations. It can be observed from our simulation result that MMSE equalizers detect signals better than the ZF equalizer even with more antenna configurations. For instance, at

the bite error rate of 6.74×10^{-4}, a 13 dB gain of SNR is achieved. Furthermore, despite its ability to nullify interferences, ZF equalizer performs just slightly better than the conventional communications with SISO antenna system because of the noise enhancement in the course of the process of an equalization of this scenario.

4.5. MIMO with ZF-SIC Equalizer

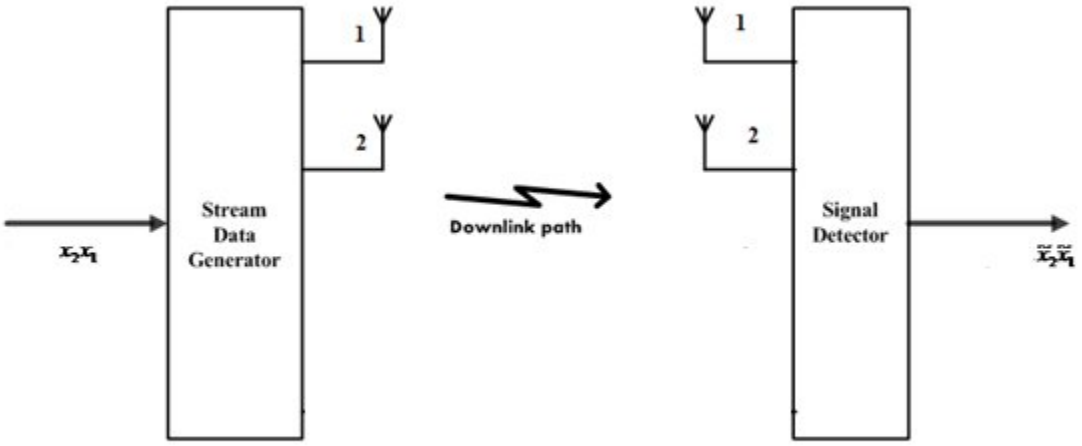

Figure 4.2. Spatially multiplexed MIMO structure.

The received signal at the respective antennas can be given as

$$y_1 = h_{11}x_1 + h_{12}x_2 + z_1$$

$$y_2 = h_{21}x_1 + h_{22}x_2 + z_2 \,. \tag{4.25}$$

In order to solve for x from the matrix representation of the received signal $y = Hx + z$, the weight matrix of the ZF linear detector with constraint $WH = I$ should be used. Then the receiver can estimate the received symbols as follows.

$$\tilde{x} = Wy = (HH^H)^{-1} H^H y \,. \tag{4.26}$$

Using ZF-SIC equalization approach, the effect of each estimated symbol is subtracted from the received signal vector. For instance, take the estimated symbol $\tilde{x}_2$ and perform the following operation:

$$\begin{aligned} r_1 &= y_1 - h_{12}\tilde{x}_2 = h_{11}x_1 + z_1 \\ r_2 &= y_2 - h_{22}\tilde{x}_2 = h_{21}x_1 + z_2 \,. \end{aligned} \tag{4.27}$$

From equation (4.27), the following matrix form representation is obtained:

$$r = hx_1 + z \ . \tag{4.28}$$

Finally the equalized symbol obtained from equation (4.28) is expressed as

$$\tilde{x}_1 = \frac{h^T r}{h^T h} \ . \tag{4.29}$$

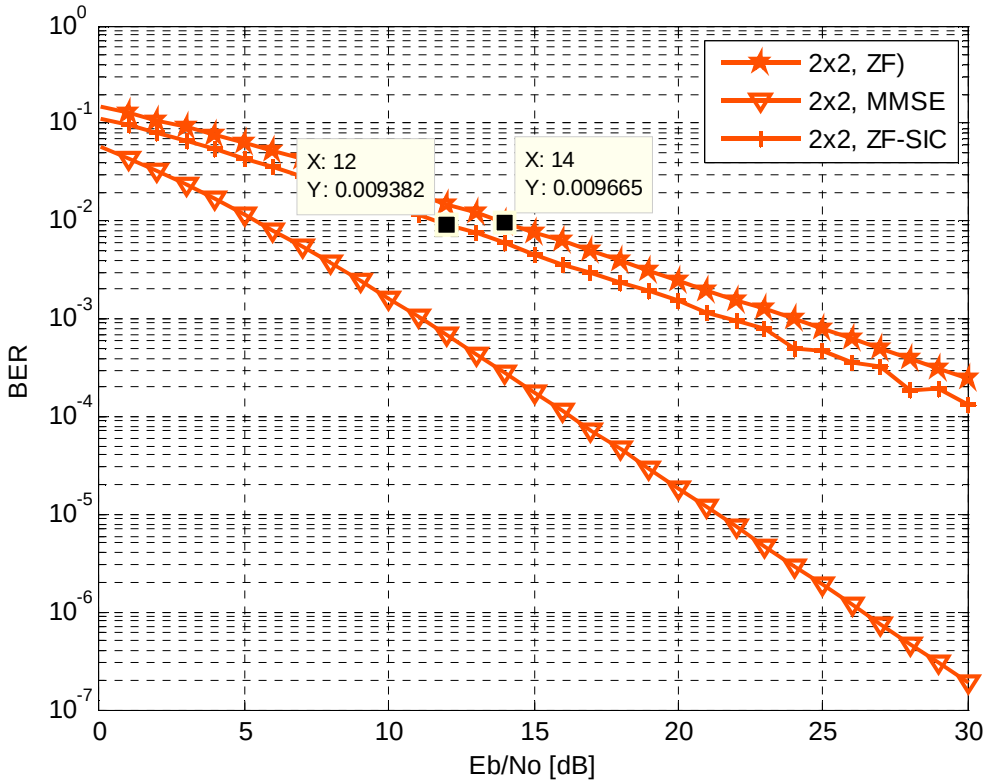

Figure 4.3. BER performances comparison for MMSE, ZF and ZF-SIC using QPSK.

The simulation result in the above plot shows the addition of successive interference cancellation results in an improvement of the ZF equalizer. For instance, at a bit error rate of 10^{-2}, it can be seen that there is an improvement of 2 dB as a result of using successive interference cancellation.

4.6. Channel Estimation at the Transmitter Side

In the previous sections, it is assumed that only the receiver can track the channel. Since a transmitter does not have direct access to its own channel, the channel information must be

estimated at the receiver side and then fed back to the transmitter side. The downside of this approach is that additional bandwidth is needed for transmitting the feedback information from the receiver to the transmitter. Moreover, the information may not be fully available or may be outdated due to the feedback delay.

The technique that is employed and compared for this channel estimation at the transmitter is a pre-MMSE equalizer versus linear MMSE and ZF at the receiver.

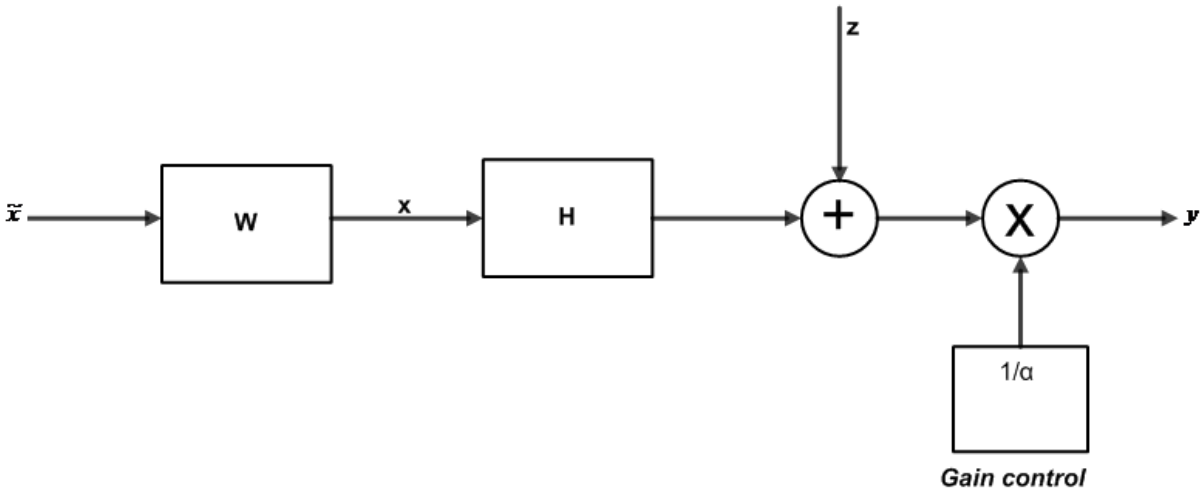

Figure 4.4. Linear pre-equalization.

Let the pre-equalizer weight matrix and the pre-coded symbol vector respectively be $W \in C^{nT \times nT}$ and $x \in C^{nT \times 1}$, where nT is the number of the transmit antennas. Given the original symbol vector for transmission $\tilde{x}$, the pre-coded symbol vector can be expressed as

$$x = W\tilde{x} . \tag{4.30}$$

For zero-forcing equalization, the corresponding weight matrix provided square channel matrix is given by the following formula as in Cho et al. (2010:381) :

$$W_{ZF} = \alpha(HH^H)^{-1}H^H, \tag{4.31}$$

where $\alpha = \sqrt{\frac{nT}{tr(H^{-1}(H^{-1}))^H}}$,which is transmitted power constraint factor after pre-equalization.

The received signal at the receiver must be divided by α via the gain control to compensate for the transmitted power amplification at the transmitter side. Then, it is given as

$$\begin{aligned} y &= \frac{1}{\alpha}(Hx + z) \\ &= \frac{1}{\alpha}(HW_{ZF}\tilde{x} + z) \\ &= \frac{1}{\alpha}(H\alpha(HH^H)^{-1}H^H\tilde{x} + z) \\ &= \frac{1}{\alpha}(\alpha HH^{-1}\tilde{x} + z) \;\; = \frac{1}{\alpha}(\alpha\tilde{x} + z) \\ &= \tilde{x} + \tilde{z}\,. \end{aligned} \tag{4.32}$$

For MMSE equalization, the weight matrix is given as

$$W_{mmse} = \alpha \times \arg_w \min E\left\{\left\|\alpha^{-1}(HW\tilde{x}+n)-\tilde{x}\right\|^2\right\}$$
$$= \alpha \times H^H (HH^H + \frac{\sigma_n^{\ 2}}{\sigma_x^{\ 2}} I)$$
$$= \alpha \times H^H (HH^H + \frac{1}{SNR} I) \ . \qquad (4.33)$$

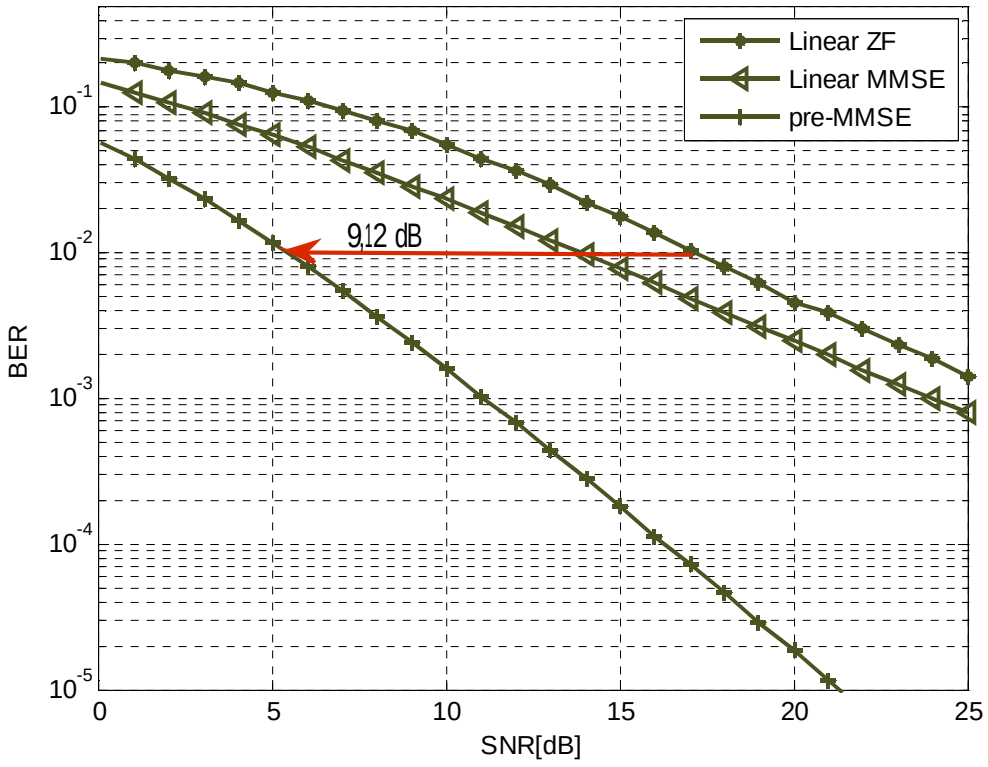

Figure 4.5. Pre-equalization versus receiver-side MMSE/ZF equalization using 16-QAM with 4×4 MIMO antennas (number of frames=100, number of packets=10000).

The figure shows the performance of channel estimation at the transmitter side with information obtained from the receiver side fed back to the transmitter. It can be seen from the simulation result that the pre-equalization technique at the transmitter side outperforms the linear equalizations at the receiver side. For example, at a bit error rate of 10^{-2} by using pre-MMSE equalization , SNR gains of 9 dB and 12 dB are achieved over using linear MMSE and ZE equalizers at the receiver, respectively. Besides, on trying to examine the performance by keeping the number of packets constant and varying the number of frame, it has been observed that there is no performance improvement, except that the processing time has increased because the payload of data over the communications network to the destination needs more processing time as the number of frame increases.

5. CONCLUSION AND FUTURE WORKS

The uplink transmission in LTE and its advanced version uses the same frame structure, the same subcarrier spacing and the same modulation parameters as the downlink. However, unlike in the downlink OFDMA subcarrier modulation where the QPSK/QAM symbols are directly modulated to the corresponding subcarriers, in the uplink subcarrier modulation, data is mapped onto a signal constellation and symbols are sequentially fed into a serial/parallel converter and then fed into an FFT block. This difference in the subcarrier modulation of the uplink SC-FDMA brings in a lower PAPR which is important for cost-effective design of end-user power amplifiers. This unique feature of SC-FDMA has led the 3GPP standardization bodies to unanimously adopt it as the uplink transmission, which later emerged as one of the radio interface technologies in IMT-Advanced standards. In addition, an uplink SC-FDMA transmission with DFDMA and LFDMA has a better PAPR performance than an OFDMA system. Even if DFDMA has a lower PAPR than LFDMA, the LFDMA system is usually implemented.

The primary objective of this thesis is to study the performances of MIMO MMSE, ZF and ZF-SIC equalizers in a Rayleigh fading channel, and the simulation results have shown that an MMSE equalizer detects signals better than a ZF equalizer. Nevertheless, an addition of successive interference cancellation can improve the performance of the ZF equalization. It is still advisable to use the ZF equalizer without the addition of SIC as a low noise power amplifier can be added at the receiver to suppress the noise enhancement that degrades the performance.

Finally, it is observed that the pre-equalization scheme on the transmitter side outperforms the receiver-side equalization. This is because using the channel feedback enables the transmitter to use variable power at a variable rate to transmit while the receiver-side equalization suffers from noise enhancement in the course of the process. Therefore, it is encouraged to use pre-equalization technique to estimate channel information, and this

work suggests an interesting avenue for further research especially to solve the bandwidth constraint to send the feedback to the transmitter in the pre-equalization techniques.

5.1. Future Works

The readers of this project ought to be briefed that all the simulations have been done in a pedestrian environment of zero mobility. But since the impact of high terminal mobility on 4G cellular networks also needs to be given a deep insight, it is recommended to anyone who is interested to continue with turbo channel coding or low-density parity-check channel coding included in their work.

REFERENCES

3GPP (2012).*3GPP Partners*: *Organizational and Market Representation Partners* [Online].3GPP Partners [cited 20.05.2012]. Available from World Wide Web: <http://3gpp.org/Partners>.

3GPP (2012). *LTE Release Freeze Dates* [Online]. Freeze Dates [cited 20.05.2012]. Available from World Wide Web: < http://3gpp.org/Releases>.

3GPP (2012).*3GPP Specification Series* [Online].Specification [cited 20.05.2012]. Available from World Wide Web: <http://3gpp.org/Partners>.

Agilent Technologies (2011). *Introducing LTE-Advanced* [Online]. USA: Agilent Technologies [cited 21.05.2012]. Available from World Wide Web: < www.agilent.com/find/4glte>.

Akyildiz, Ian, David Gutierrez-Estevez & Elias Reyes (2010). *The Evolution to 4G Cellular Systems: LTE-Advanced*. Atlanta: Elsevier.

Barry, John, Edward Lee & David Messerschmitt (2003). *Digital Communication*. 3rd Ed. USA: Kluwer Academic Publishers.

Cho, Yong, Chung Kang, Jaek Kim & Won Yang (2010).*MIMO OFDM Wireless Communications with Matlab*. Singapore: Wiley

Cisco Visual Networking Index (2010). *Global Mobile Data Forecast Update* [Online].

San Francisco: Cisco [cited 31.05.2012]. Available from the Internet:

<http://www.cisco.com/en/US/solutions/collateral/ns341/ns525/ns537/ns705/ns827/white_paper_c11-520862.html>.

Hanzo, Lajos, Li Wang, Ming Jiang &Yosef Akhtman (2011). *MIMO OFDM for LTE, WiFi and WiMAX: Coherent versus Non-coherent and Cooperative Turbo-Transceivers.* Chichester: Wiley.

Haykin, Simon (2001). *Communication Systems*.4th Ed. USA: Wiley.

Holma, Harri & Antti Toskala (2009). *LTE for UMTS-OFDMA and SC-FDMA Based Radio Access*. Chippenham: Wiley.

Khan, Farooq (2009). *LTE for 4G Mobile Broadband: Air Interface Technologies and Performance*. New York: Cambridge University Press.

Koivo, Heikki & Mohammed Elmusrati (2009). *Systems Engineering in Wireless Communications*. Chippenham: Wiley. 298-301p.

Li, Qinghua, Bruno Clerckx, David Mazzarese, Guangjie Li, Moon-il Lee, Wookbong Lee & Zexian Li (2009). *MIMO Techniques in WiMAX and LTE: A Feature Overview*. IEEE Communications Magazine, 86–92.

Maravedis (2010). *The 4G (LTE and WiMAX) Deployment and Subscriber Forecasts 2011-2014* [Online]. Montreal: Maravedis [cited 23.05.2012]. Available from the Internet :< http://www.maravedis-bwa.com/en/reports#report-226>.

Nakamura, Takehiro (2009).*Proposal for Candidate Radio Interface Technologies for IMT-Advanced Based on LTE Release 10 and Beyond (LTE-Advanced)* [Online]. Beijing: 3GPP IMT-Advanced Evaluation Workshop [cited 07.06.2012]. Available from the Internet: <http://3gpp.org/IMG/pdf/2009_10_3gpp_IMT.pdf>.

Proakis, John G. (2000). *Digital Communications*. 4th Ed. New York: McGraw Hill.

Ross, Sheldom M. (2010). *Introduction to Probability Models*. 10th Ed. California: Elsevier.

Schulze, Henrik & Christian Lüders (2005). *Theory and Applications of OFDMA and CDMA: Wideband Wireless Communications*. Chichester: Wiley.

Sklar, Bernard (2001). *Digital Communications: Fundamentals and Applications*. 2nd Ed. New Jersey: Prentice Hall PTR.

Tse, David & Pramod Viswanath (2005). *Fundamentals of Wireless Communication*. New York: Cambridge University Press. ISBN-10: 0521845270.

APPENDICES

Appendix 1. Proof of QPSK BER in a Rayleigh Fading Channel

Use the following definitions of *erfc* and *erf* functions:

1. $erfc(x) = \frac{2}{\sqrt{\pi}} \int_{\pi}^{\infty} e^{-t^2} dt$;
2. $erf(x) = \frac{2}{\sqrt{\pi}} \int_{0}^{\pi} e^{-t^2} dt$;
3. $\frac{d}{dx} erf(x) = -\frac{2}{\sqrt{\pi}} e^{=x^2}$.

Using the integration by-parts, the following definite integral can be solved:

$$\int erfc(x)dx = xerfc(x) + \int x \frac{2}{\sqrt{\pi}} e^{-x^2} dx$$

$$= xerfc(x) - \frac{1}{\sqrt{\pi}} e^{-x^2} .$$

The following steps can also be used:

$$\frac{d}{dx} erfc(\sqrt{x}) = \frac{-1}{\sqrt{\pi}} e^{-x} x^{-1/2} \text{ and } \frac{d}{dx} erf(\sqrt{x}) = \frac{1}{\sqrt{\pi}} e^{-x} x^{-1/2} .$$

Then the following integral can be solved by parts:

$$\int erfc(\sqrt{x}) e^{-\frac{x}{a}} dx = -aerfc(\sqrt{x}) e^{-\frac{x}{a}} - \int (-a) e^{-\frac{x}{a}} (-1) \frac{1}{\sqrt{\pi}} e^{-x} x^{-1/2} dx$$

$$= -aerfc(\sqrt{x}) e^{-\frac{x}{a}} - \frac{a}{\sqrt{\pi}} \int e^{-\frac{x}{a}} e^{-x} x^{-1/2} dx$$

$$= -aerfc(\sqrt{x}) e^{-\frac{x}{a}} - \frac{a}{\sqrt{\pi}} \int e^{-x(\frac{a+1}{a})} x^{-1/2} dx$$

$$= -aerfc(\sqrt{x})e^{-\frac{x}{a}} - \frac{a}{\sqrt{\pi}}\int e^{-u}(\frac{a}{a+1})^{-1/2}u^{-1/2}(\frac{a}{a+1})du$$

$$= -aerfc(\sqrt{x})e^{-\frac{x}{a}} - \frac{a}{\sqrt{\pi}}(\frac{a}{a+1})\int e^{-u}u^{-1/2}du.$$

$$= -aerfc(\sqrt{x})e^{-\frac{x}{a}} - \frac{a}{\sqrt{\pi}}.\sqrt{\pi}(\sqrt{\frac{a}{a+1}})erf(\sqrt{u})$$

$$= -aerfc(\sqrt{x})e^{-\frac{x}{a}} - a(\sqrt{\frac{a}{a+1}})erf(\sqrt{u})$$

$$= -aerfc(\sqrt{x})e^{-\frac{x}{a}} - a(\sqrt{\frac{a}{a+1}})erf(\sqrt{\frac{a}{a+1}}\sqrt{x}).$$

Using the above demonstration, the bit error rate of QPSK modulation in a Rayleigh fading channel is derived as

$$P_b = \int_0^\infty \frac{1}{2}erfc(\sqrt{\beta}) \times P(\beta)d\beta$$

$$= \frac{1}{2\overline{\beta}}\int_0^\infty erfc(\sqrt{\beta}) \times e^{-\frac{\beta}{\overline{\beta}}}d\beta$$

$$= \frac{1}{2\overline{\beta}}[\overline{\beta}erfc(\sqrt{\beta})e^{-\frac{\beta}{\overline{\beta}}} + \overline{\beta}\sqrt{\frac{\overline{\beta}}{\overline{\beta}+1}}erf(\sqrt{\frac{\overline{\beta}}{\overline{\beta}+1}}\sqrt{\beta})]|_\infty^0$$

$$= \frac{1}{2}(1 - \sqrt{\frac{\overline{\beta}}{\overline{\beta}+1}})$$

$$= \frac{1}{2}(1 - \sqrt{\frac{E_b/N_0}{(E_b/N_0)+1}}).$$